Techno-economic and exergy analysis of polygeneration plant for power and DME production with the integration of chemical looping CO2/H2O splitting

Techno-economic and exergy analysis of polygeneration plant for power and DME production with the integration of chemical looping CO_2/H_2O splitting

Azharuddin Farooqui*[¥°], Felice Di Tomaso*, Archishman Bose[$], Domenico Ferrero*, Jordi Llorca[¥], Massimo Santarelli*

* Energy Department (DENERG), Politecnico di Torino, Corso Duca Degli Abruzzi 24, Torino 10129, Italy

[¥] Institute of Energy Technologies, Department of Chemical Engineering and Barcelona Research Center in Multiscale Science and Engineering, Universitat Politècnica de Catalunya, EEBE, Eduard Maristany 10-14, Barcelona 08019, Spain

[$] Marine and Renewable Energy Research (MaREI) Centre, Environmental Research Institute, School of Engineering and Food Science, University College Cork, Lee Road, Cork, T23 XE10, Ireland

° Corresponding author.

Abstract

In this paper, we present a novel polygeneration plant with carbon capture for the combined power and dimethyl ether (DME) production. The plant layout integrates a chemical looping CO_2/H_2O splitting (CL) unit producing syngas (CO and H_2) for the DME synthesis using the exhaust gases of an oxyfuel power cycle. The primary power is generated by oxy-combustion of syngas generated by the reduction of the metal oxide in the reduction unit of the CL redox cycle with incoming natural gas. The oxyfuel power plant also generates steam for combined power production with two streams Rankine cycles. The aim of the present work is to assess the process on the basis of energy and exergetic efficiency and economic performance of the integrated CL unit for combined power and DME production. The integration proposed resulted in a production of 103 MW_e and 185.6 ton/day (2.15 kg/s) of DME. The corresponding energy and exergetic efficiency was 50.2% and 45%, respectively. A discounted cash flow analysis was performed to evaluate the profitability of the process. With a carbon credit of $80/tonne, the plant would be able to meet the current electricity with carbon capture and DME prices of $50/MWh and $18/GJ respectively. The economic analysis provided information on the main economic drivers associated with the high capital investment in the process plant with individual sub-systems. The analysis highlighted the strong potential of integrating chemical looping CO_2/H_2O splitting for syngas production into polygeneration systems to increase the overall efficiency while reducing the cost of carbon capture.

Keywords: CO_2/H_2O splitting, Chemical looping, Polygeneration, Oxyfuel combustion, Dimethyl-ether (DME), carbon capture.

1. Introduction

CO_2 emissions from the energy sector – mainly from the combustion of fossil fuels – comprise the largest fraction of the global anthropogenic GHG emissions, representing 58% of the total emissions, as of 2014 [1]. The quest to meet the never-ending energy demand and the rise of emissions is leading to the search for innovative technologies and non-petroleum based alternative fuels which would help in restricting the global warming to 1.5^{o}C above the pre-industrial temperatures (new target set by the recent report by Intergovernmental Panel on Climate Change (IPCC), 2018) [2]. Among the multiple pathways proposed for the reduction of anthropogenic emissions of CO_2, Carbon capture and utilization (CCU) to convert captured CO_2 into valuable products have recently gained much focus as an alternative to Carbon Capture and Storage (CCS) [3–5]. CCU is not only complementary to CCS in some respects but also provides multi-product outputs through the recycling and reuse of the captured CO_2 in several synthesis processes [6–9]. Carbon capture in power plants comes with huge energy penalty and loss of efficiency. For example, in oxyfuel natural gas combined cycle (NGCC) power plants, Air separation unit (ASU), used to produce pure oxygen for combustion results in the decrease the efficiency of the conventional NGCC by as much as ~13% [10]. Multiple studies have been proposed to gain this loss of efficiency by alternate methods like the use of ion transport membranes (ITM) for oxygen separation instead of ASU [11] or recycling exhaust flue gas to run a redox cycle with a metal oxide [12]. Polygeneration systems, which can combine efficiently multiple utility outputs (e.g., electrical power, chemicals, fuels etc.) from one or more input in a single system, provide an interesting option for CCU [13]. Besides the potential to gain significant efficiency and local use of the captured CO_2, suitable integration and synergy between different processes also ensure higher flexibility of operation. This would allow varying between the share of products according to their value, for example, related to fluctuating market prices [14]. Multiple configurations of polygeneration systems integrated with CO_2 capture processes have been reported in the literature. Li et al. [15] modelled a polygeneration plant with CO_2 capture for production of power and synthetic natural gas, the proposed arrangement achieving a lower life-cycle energy use and GHG emission with respect to the ultra-supercritical coal power plant. Bose et al. [16] studied a cost-effective production of urea and power combined with CCS using coal gasification. Jana et al [17] reported the improved sustainability through life cycle assessment for a rice-straw based power, ethanol, heating and cooling polygeneration power plant. Huang et al [18] highlighted both energetic and economic benefit of a coal based polygeneration system for power and methanol production as opposed to single coal-to-methanol or coal-to-power systems. Salkuyeh [19] proposed a novel methanol, DME and power production plant from the combined use of coal and natural gas via chemical looping combustion that not allowed complete carbon captured at improved efficiency.

Most polygeneration systems designed or proposed till date have employed coal as the fuel [13]. However, oxyfuel combustion using gaseous fuels like natural gas and biomethane has been shown to be the most promising among the low emission technologies (LETs) [12]. Above such, innovative methods for the use of natural gas are being proposed to improve upon the efficiency of natural gas combined cycle power plants, which can reach an efficiency of as high as 57% [20]. One such innovative technology is the chemical looping CO_2/H_2O splitting cycle using methane reduction, to produce CO and H_2 [12]. This indeed forms an interesting alternative to the solar

thermochemical redox cycle, which has gained attention for CO_2/H_2O splitting to produce syngas (CO/H_2) utilizing the successful demonstration of water splitting by oxygen careers [21–24]. For the solar-thermochemical redox cycle, the metal oxide (also called as oxygen career (OC)) undergoes endothermic thermal reduction (TR) step, thus requiring a very concentrated heat, usually provided by solar energy under a very high vacuum pressure [25,26]. In the second step, the reduced oxygen carrier undergoes oxidation by the incoming CO_2/H_2O producing CO/H_2, thereby ensuring a continuous cycle. The second step is exothermic in nature and operates at near atmospheric pressures and lower temperature than the thermal reduction creating a temperature and pressure swing between the two steps. Fuel reduction with methane, however, results in the reduction step to operate at near atmospheric conditions, thus, avoiding pressure swing operation. Furthermore, it lowers the reduction temperature, preventing a large temperature swing between the two-steps. An added advantage is gained from the production of syngas in both the steps of redox cycle [12,27,28]. Chemical looping (CL) cycle driven by methane reduction (which can be replaced by bio-methane in future), has an added benefit of being able to operate round the clock, unlike solar driven cycles that are constrained by the fluctuation of the solar energy source. A basic schematic of the methane-driven chemical looping CO_2/H_2O splitting cycle is shown in Figure 1.

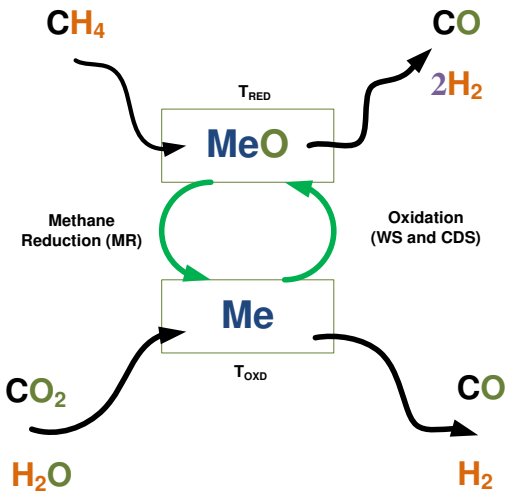

Figure 1. A representative schematic of chemical looping syngas production through methane reduction and corresponding splitting of water and carbon dioxide.

Multiple metal oxide redox pairs have been studied for the CL application [25,26,29]. Among the materials, cerium (IV) oxide (CeO_2) is considered to be one of the most promising for the present application due to its strong ability to undergo cyclic redox reactions while retaining its chemical and structural properties together with high resilience to mechanical stress and agglomeration resistant [30]. Ceria reduction by methane has been investigated by Warren and Scheffe [31]. Results indicate that CeO_2 undergoes complete reduction to Ce_2O_3 above 900°C. Accordingly, the CeO_2/Ce_2O_3 redox pair with reduction of CeO_2 in the presence of methane, and subsequent oxidation with CO_2/H_2O can be described in terms of the following equations (1-3).

$$\text{Methane reduction (MR): } 2CeO_2 + CH_4 \rightarrow Ce_2O_3 + CO + 2H_2 \quad (1)$$

$$\text{Water-splitting(WS): } Ce_2O_3 + H_2O \rightarrow 2CeO_2 + H_2 \quad (2)$$

CO_2-splitting (CDS): $Ce_2O_3 + CO_2 \rightarrow 2CeO_2 + CO$ (3)

By optimally combining the ratio of water and CO_2 in the inlet gas mixture to the oxidation reactor and the temperature of reaction, the desired composition of syngas can be obtained, to be subsequently utilized for production of chemicals ((H_2/CO: 1.79) methanol [32,33], (H_2/CO: 2.1) jet fuels [34] and naphtha [34–36], (H_2/CO: 1.76) kerosene and gasoil [36] etc.) through industrial processes.

Dimethyl Ether (DME) is one of the most attractive candidates as a synthetic fuel due to its similarity with diesel. Even though DME has a lower LHV than conventional diesel and its use requires pressurization to maintain it in a liquid state at ambient conditions, its physical properties and chemical structure make it a very interesting fuel. Low NO_x, limited hydrocarbon (HC) and almost no SO_x and particulate emissions during the combustion [37,38], are added advantages of its use. However, challenges including the need for re-design of the injector and fuel pump systems, compatibility of sealant materials are current limitations to the complete replacement of diesel by DME in conventional compression ignition engines [37]. In this regard, blending of DME with conventional automotive fuels have been advocated as an important strategy to improve both applicability and economic viability of DME in the short term [37,39]. Furthermore, the unique physico-chemical properties of DME would allow its use as a raw material for the synthesis of aromatics, gasoline, olefins and other chemicals besides direct use as an alternative fuel or a substitue to conventional refrigerants [40]. It is to highlight that DME also gained attention in recent times due to its physicochemical properties are similar to liquid petroleum gas (LPG) giving the chance to retrofit the LPG based automotives [41]. However, being a synthetic fuel, the price of DME would be constrained by the cost of feedstock, including its transportation, in the present case, natural gas [42]. As per long term future predictions, both diesel and natural gas prices have been projected to rise at an euqal steady rate [43,44]. This, even though would allow the relative economic competitiveness of DME with respect to diesel, would increase its cost nevertheless in future. In this regard, research and development for sourcing methane from biomass as biomethane could potentially improve both environemntal and economic volatility associated with DME synthesis.

DME synthesis is generally classified as i) two-step process (indirect) which uses hydrogenation to produce methanol and then dehydration to DME ii) the second method is one-step (direct) process reported to be more efficient which uses bi-functional catalysts. Both the pathways are commercially viable technology and invested by companies such as Haldor Topsoe, Korea Gas Corporation, Air products, JFE Holdings, Toyo, MGC, Lurgi and Udhe [45,46]. Synthesis of DME using syngas (CO and H_2) from CO_2/H_2O splitting can, therefore, present an interesting pathway for the production of clean fuels using an unconventional process [47,48]. Interestingly, the production of DME by the single step process has been shown to significantly improve the overall process efficiency with respect to both methanol production or the indirect DME synthesis process, providing additional economic impetus to its commercial application [49].

Alternative methods to produce syngas by the chemical looping processes has been reported such as chemical looping reforming (CLR), autothermal reforming and chemical looping partial oxidation of methane (CLPOM) [50,51]. CLR and autothermal reforming usually operate at a lower

temperature of 800-900°C that produces H_2/CO ratio of 2.8-4.8 and 1.8-4.0 respectively with a higher concentration of CO_2/H_2O at the outlet stream. While syngas production by CLPOM needs a temperature above 1300°C with H_2/CO of 1.7-1.8 and also has lower H_2O/CO_2 in the product [52]. This makes CLR more suitable for Fischer-Tropsch synthesis for methanol or hydrogen production. However, a novel process of generation of syngas from the exhaust stream and re-use within the power plant for producing additional power has been shown to be a viable alternative to improve the efficiency with 100% carbon capture [12]. Indeed, within a polygeneration scheme, the use of syngas for synthetic fuel production becomes an imperative option. Hankin and Shah [49] in an study explored the process of DME and methanol synthesis from CO_2 and H_2O. Syngas is produced by water electrolysis and solid oxide electrolysis for CO where all the processes such as DME, methanol synthesis, electrochemical electrolysis and solid oxide electrolysis for CO are investigated by assumption of chemical equilibrium. Salkuyeh and Adam II [19] proposed a polygeneration scheme which combines the coal gasification, natural gas reforming by chemical looping processes such as gasification and combustion to produce power, methanol, and DME. The system was tested with iron oxide and nickel oxide oxygen career for chemical looping processes with different gains based on the operability of the system. The path for syngas production as feedstock DME was investigated.

However, till date, as per the knowledge of the authors, no polygeneration system which integrates the chemical looping CO_2/H_2O splitting (CL) with fuel reduction step and DME and power production have been studied for utility-scale. In this work, an oxyfuel natural gas combined cycle power plant integrated with CL CO_2/H_2O splitting and DME production has been proposed (OXYF-CL-PFG) with a detailed techno-economic, exergetic and environmental assessment. The exergetic study was carried out for the proposed OXYF-CL-PFG layout to identify the sources of irreversibility, with which the proposed layout could be improved and optimized. The analysis includes power production, fuel production, and power consumption, exergy analysis, economic estimation along with the net present value (NPV) with different carbon credit scenarios, as well as efficiency and percentage of carbon captured and recycled.

2. Process and plant description

The proposed polygeneration scheme is an oxyfuel natural gas fed combined cycle power plant integrated with a chemical looping CO_2/H_2O splitting unit (CL) for power and DME production (OXYF-CL-PFG) shown in Figure 2. To maintain the simplicity of analysis, the gas pre-treatment including sulphur removal has been assumed to have occurred upstream [53] The clean natural gas is sent to the chemical looping (CO_2/H_2O) splitting unit where it is converted into a hydrogen-rich syngas by the simultaneous reduction of ceria. The produced syngas is sent to an oxyfuel unit where it is combusted with pure oxygen from an ASU. The hot combustion products, primarily comprising H_2O and CO_2 are firstly expanded in a gas turbine and then sent in a heat recovery steam generation unit (HRSG). Here, the surplus heat is exploited to produce superheated steam for power production in a bottoming steam cycle. Finally, a water condenser partially separates carbon dioxide and water. The large part of the separated CO_2 can be sequestrated for storage or used in other processes, while another fraction together with steam is sent to the chemical looping CO_2/H_2O (CL) unit. In the CL unit, both H_2O and CO_2 are dissociated to H_2 and CO in an oxidation reactor by the reduced ceria from the reduction reactor. The produced syngas from the oxidation reactor is used for DME

synthesis. The diluted DME, resulting thus, is cleaned in a distillation unit (or clean-up unit), additionally producing a secondary fuel stream of methanol. In the following sub-sections, the methodology adopted for the presented work, along with more details on each unit and their integration are described.

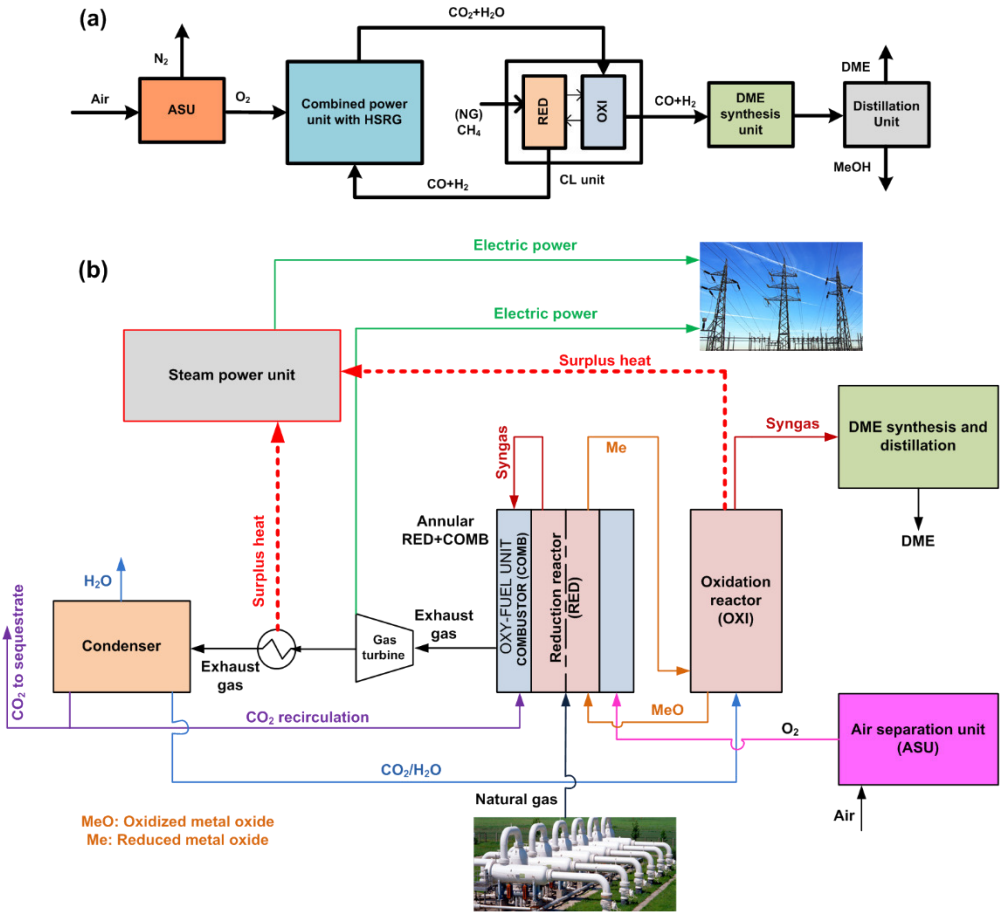

Figure 2: General concept of integration of oxy-fuelled power unit with chemical looping (CO_2/H_2O) splitting unit and DME production process (a) block diagram (b) process flow diagram

2.1 Simulation Methodology

The polygeneration plant has been modelled by combining mass and energy balance equations. As per the detailed plant layout proposed in Figure 3. Simulations were performed using the commercial software Aspen Plus v8.8. The characteristic components of the system are the integrated combustor of the oxyfuel unit and the reduction reactor of the CL unit and oxidation reactor, the DME synthesis reactor, the DME distillation columns, and the ASU apart from the standard components of the plant, such as heat exchangers, pumps, compressors, and turbines. The entire modelling was performed with the assumption of chemical equilibrium with the exception of the DME reactor, for which a kinetic approach has been used. Therefore, RGIBBS reactor blocks were used for modelling the oxidation and reduction reactors of the CL unit, as well as the combustor of the oxyfuel unit. The distillation unit and air separation columns were modelled using the RADFRAC column. The DME reactor was simulated with an RPLUG reactor using the Langmuir-Hinshelwood Hougen-Watson (LHHW) kinetic model. During the simulation of this

component, the Soave-Redlich-Kwong (SRK) EOS model was utilized, which is usually applied to binary components [54]. Graaf et al. [55] demonstrated that the chemical equilibrium of the methanol reaction and water gas shift (WGS) reaction can be well described at high-pressure by using the SRK-EOS model. More details on the modelling approaches followed for the main components of the plant are given in section 2.1-3.

The material streams used in the model involve conventional and solid components. The Peng-Robinson-Boston-Mathias (PR-BM) property method was used for conventional components, as this approach was recommended for hydrocarbon processing applications such as gas processing, refinery, and petrochemical processes [56–58]. This method uses the Peng-Robinson cubic equation of state combined with the Boston-Mathias alpha function for all the thermodynamic properties [57]. The oxygen carriers (CeO_2/Ce_2O_3) used for the chemical looping simulation were implemented as conventional pure solid components. For this type of streams, the Barin equation was used [59,60]. The main hypotheses used in the modelling phase are summarized in Table 1. CLN-CO_2, CLN-DME, and CLN-MeOH are the columns used in the distillation unit.

Table 1. Main assumptions and hypothesis used in the process simulation.

Natural gas	Composition (std.vol%): 93.1% CH_4, 3.2% C_2H_6, 1.6% N_2, 1.1% C_3H_8, 1.0% CO_2; LHV=47.1 MJ/kg [61];	
Oxidation and reduction reactors	Model: RGIBBS, no heat losses; 10°C drop for ceria recirculation from OXI to RED was assumed in order to assess heat losses; Model: RGIBBS;	
Combustor	Model: RGIBBS; ΔP=0.2 bar, no heat losses;	
Compressors, pumps and turbines	$\eta_{is,comp}$=0.9, $\eta_{mech,comp}$=0.98, $\eta_{is,pump}$=0.9, $\eta_{driver,pump}$=0.90, $\eta_{is,turb}$=0.9, $\eta_{mech,turb}$=0.98;	
Oxygen carrier	Solid ceria: CeO_2/Ce_2O_3, diameter=100 μm; Temperature drop of 20°C during ceria recycling from OXI to RED;	
DME reactor	Model: RPLUG multi-tube reactor, Operation: T=250°C P=50 bar;	
Heat exchangers	ΔT_{min}=10°C;	
Distillation unit	Model: RADFRAC, Reboiler type: Kettle.	
CLN-CO_2	CLN-DME	CLN-MeOH
P=10 bar	P=9 bar	P=2 bar

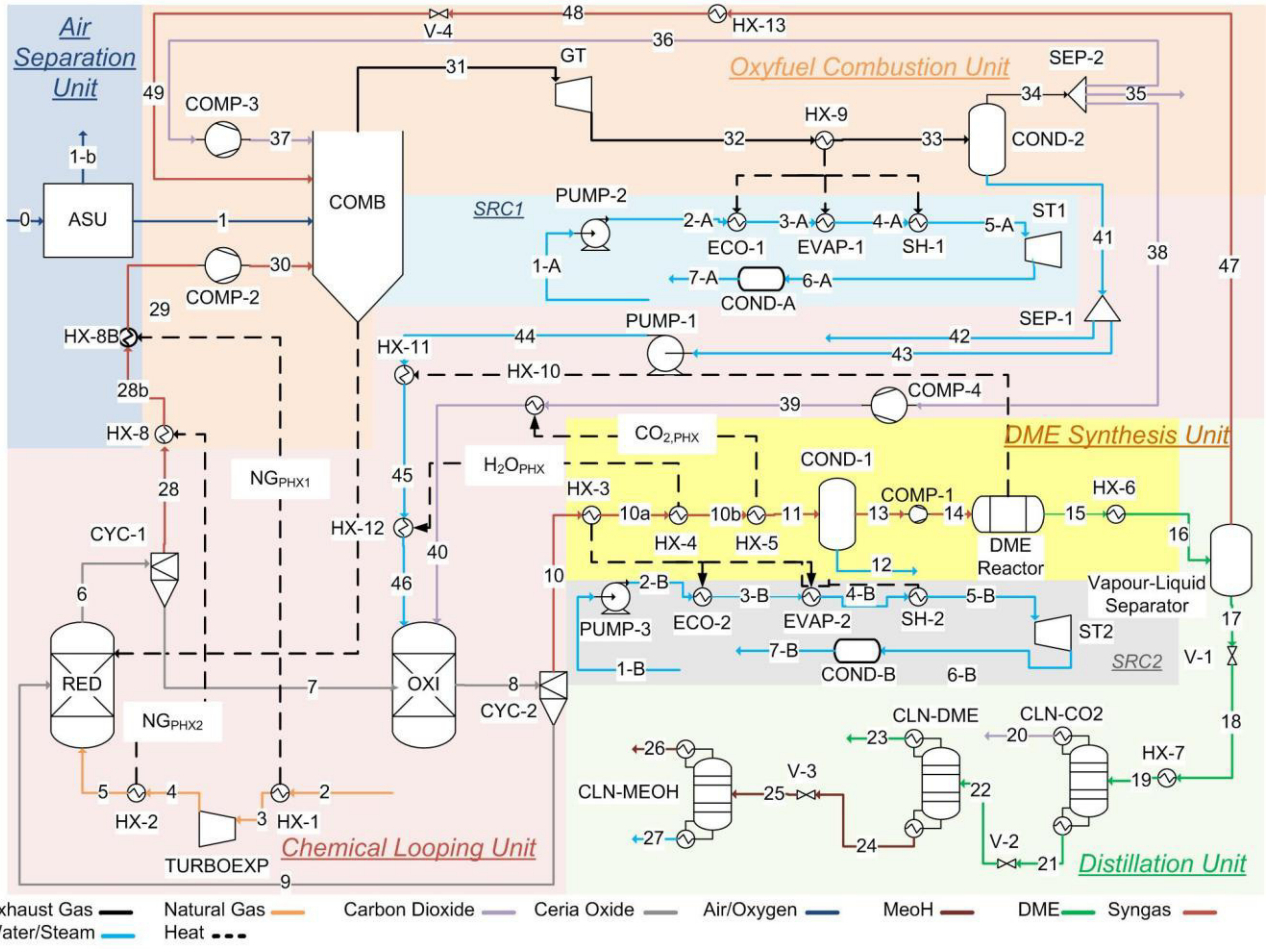

Figure 3. Detailed polygeneration plant layout OXYF-CL-PFG.

2.2 Polygeneration plant units

2.2.1 Chemical looping CO_2/H_2O splitting unit (CL unit)

The chemical looping unit consists of two interconnected reduction reactor (RED) and the oxidation reactor (OXI) operating at 2 bar with the circulating oxygen carrier pair (CeO_2/Ce_2O_3). The pre-cleaned natural gas, at a grid pressure of 70 bars (stream 2) [62] is heated up at 290°C and expanded to 2 bar via the turbo-expander (TURBOEXP). Table 1 lists the composition of natural gas at the inlet to the plant (without H_2S). The preheating is necessary to prevent an outlet temperature of the natural gas (stream 4) from the turbo-expander lower than 0°C. After the expansion of the natural gas, it is heated to 890°C (stream 5) and fed to the RED. For the endothermic reduction reaction, external heat is mandatory to maintain the reaction temperature. Ceria reduction by methane occurs above 900°C to achieve full conversion to CO and H_2 as well as a reduction to Ce_2O_3 [31]. From the thermodynamic studies, it was found that 40 to 60% excess flow of methane is required to ensure complete conversion of OC below 950°C. It was also found that the most suitable methane to ceria flow ratio (CH_4/CeO_2) for the reduction reactor was 0.7 instead of the stoichiometric ratio of 0.5. Here CeO_2 (stream 9), at an inlet temperature of 1312°C as a result of the exothermic oxidation reaction, is completely reduced with natural gas, producing a syngas in a 2:1 H_2/CO ratio (reaction 1) and unreacted natural gas [12]. As for the external heat source to sustain the reaction in the RED, it has been proposed to use a part of the heat generated in

the oxyfuel combustion chamber. To this end, a reduction reactor thermally integrated with the oxyfuel combustion chamber was proposed utilizing an annular combustion chamber design already analyzed by Khan and Shamim [63] (see Figure 2 (b)). The hot syngas (stream 6) produced in RED exits it at 900°C and is separated from the solid (stream 7) by a cyclone (CYC-1), cooled and sent to the oxyfuel unit. The reduced ceria is fed, without an intermediate heat recovery, into the OXI where it is then oxidized (reactions 2 and 3) by a gas mixture coming from the oxyfuel unit. The gas mixture of 60% H_2O and 40% CO_2 (stream 40 and 46) is necessary to ensure an H_2:CO ratio of 1:1, ideal for DME production, as described in section 3. It is observed that in order to achieve a full oxidation of Ce_2O_3, a 60% excess of the gas mixture is required. Before the oxidation, both water and carbon dioxide is compressed at the operating pressure of OXI (2 bar), respectively with a pump (PUMP-1) and a compressor (COMP-4), and heated up at 500°C. Since the reactions in the oxidation reactor are exothermic and the reactor itself is set as adiabatic, the outlet temperature of the reactor goes to 1322°C. The hot syngas produced is separated from the oxidized ceria by the cyclone separator (CYC-2), cooled down (stream 10, 10a, 10b, 11) and sent to the DME unit, while the solid stream is re-circulated back for a new reduction cycle (stream 9).

2.2.2 Air separation unit (ASU)

The ASU consists of a cryogenic distillation unit able to produce 99.99% pure O_2. The schematic of the ASU layout is shown in Figure 4. The air is separated into two thermally interconnected distillation columns, HP-COL and LP-COL, which work at 5 and 1.2 bar respectively [64–66]. The overall refrigeration is driven by the expansion from high pressure (30 bar) of the compressed air (stream 6-C and 7-C, which become 14-C and 16-C respectively, after cooling down in HX-2C) through the VALVE-2 and the TURBOEXP-2C. The inlet air (1-C) is compressed at 6.3 bars by the compressor COMP-1C and separated in two streams (4-C and 8-C) by the splitter SPLIT-1C. The stream 8-C is cooled down (becoming 9-C in the figure) in the exchanger HX-2C by the cold products (steam 19-C) of the LP-COL and then is sent to the HP-COL. The HP-COL is a 40 stages distillation column which produces N_2 -rich gaseous (stream 12-C) from the top and an O_2-rich liquid stream (stream 10-C) from the bottom. The latter stream is further cooled down through Joule-Thomson effect in the valve VALVE 1-C and fed in the 56 stage low-pressure column. The low-temperature air streams 15-C and 17-C, together with the rich-in O_2 liquid stream 11-C, provide the necessary refrigeration in the LP-COL to obtain pure N_2 (stream 20-C) from the top and from the bottom condenser the pure O_2 (stream 18-C) is produced. The latter is pumped by the PUMP-1C at the operational condition of the combustor (26 bar) in the oxyfuel unit and heated in the HX-2C to 80^{o}C. The stream data is listed in Table S1 of the supplementary data file.

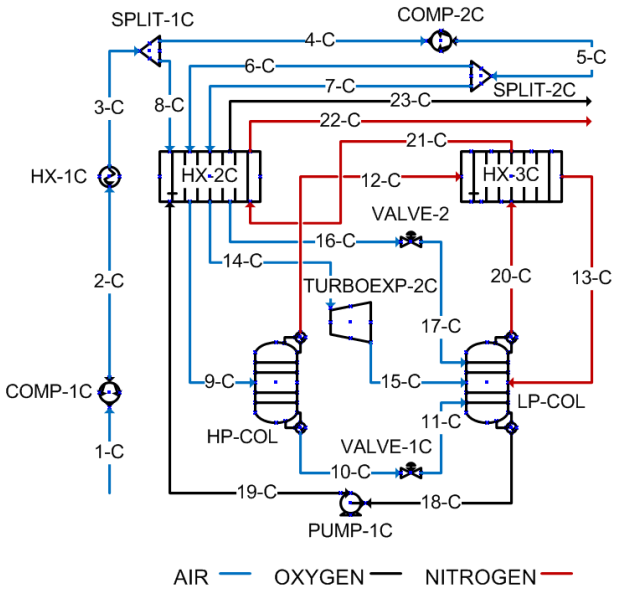

Figure 4. Detailed layout of the air separation unit

2.2.3 *Oxyfuel combustion unit*

In this unit, combustion of syngas is performed with oxygen instead of air. This eliminates the presence of nitrogen in the exhaust gases that would have affected the subsequent CO_2 separation process. Another advantage is a substantial reduction in thermal NO_x due to the absence of nitrogen [67].

The primary unit of the oxyfuel unit is the combustor (COMB), where the syngas from the reduction (stream 30) and the non-condensable gases from the clean-up unit (stream 49, mainly CO_2 with CO and H_2) are burnt with a 5% excess oxygen stream derived from the ASU (stream 1). The temperature control within the COMB is maintained by recycling a part of the captured CO_2 (Stream 36). The recirculation ratio was set so as to achieve a combustor outlet gas temperature of 1377°C in agreement to the limits of the turbine inlet temperature of commercial gas turbines as stated and selected from literature [14,68–70]) while simultaneously providing the required heat sustain the ceria reduction reaction in the RED. The CO_2 and syngas streams entering the COMB are compressed to 26 bar with two two-stage compressors (COMP-2 and COMP-3). The flue gas exiting the combustion chamber is firstly expanded in a two-stage gas turbine GT (26 bar to 5 bar and 5 bar to 1.05 bar) and then sent to the heat recovery steam generator (HX-9) for the generation of steam for the steam power cycle SRC1. More details on the steam power cycle are given in section 2.2.4. Finally, the CO_2 from the exhaust gas is separated from the water in a condenser (COND-2), generating highly pure CO_2 stream that is split into three parts. One part is recirculated to the combustor (stream 36), one is sent for sequestration or other applications (stream 35) and the last part (stream 38) is sent to the oxidation reactor for dissociation (OXI).

2.2.4 *Steam power cycle*

Two steam Rankine cycles (SRC1 and SRC2) are included in the system layout. The extra heat available within the polygeneration system is exploited to produce steam by heat recovery steam generators (HRSGs), which expands in steam turbines to generate power. The turbines and the

HRSGs were modelled as simple units, without reheating or multi-pressure systems. In fact, as the primary objective of the present study is to understand the benefits deriving from polygeneration by integration of a chemical looping unit in a conventional oxyfuel plant, the optimization of the system was not further considered. The SRC1 uses the heat of the flue gases from the oxyfuel unit (stream 32) to produce super-heated steam (125582 kg/h) at 150 bar and 550°C (stream 5A), generating an electrical power of around 44 MW while expanding in the turbine (ST1). The SRC2 uses the extra heat from the chemical looping unit to produce a smaller flow of steam (8305 kg/h) at the same condition as that of stream 5A (stream 5B), generating 3 MW in ST2. The reason for the choice of two HRSGs connected to two different steam cycles is to ensure flexible operation by minimizing the influence of DME and power production over each other.

2.2.5 DME synthesis unit

In this unit, the syngas produced in the oxidation reactor (stream 10) is converted into liquid fuel within the catalytic reactor. Before the syngas is fed to the DME reactor, it undergoes condensation (COND-1) to completely remove H_2O at atmospheric pressure. The operating conditions of the DME reactor have been selected from the work of Pozzo et al. [71] fixing the pressure at 50 bar and the temperature at 250 °C. In order to reach the operating pressure of the reactor, the dried syngas (stream 13) is compressed by a three-stage compressor at 50 bar (COMP-1). The DME reactor is a fixed bed reactor which is kept at the constant temperature of 250°C by a water-jacket cooler used for saturated steam generation at 2 bar (stream 44) for the oxidation (OXI) reactor.

The DME reactor was considered as a multi-tube fixed bed reactor. Each tube contains the dual catalyst (physically mixed) with a bed voidage of 0.45. The total density of the catalyst particles is an average of the density of the two catalysts, $Cu/ZnO/Al_2O_3$, and γ-Al_2O_3, used in the 1:2 optimal ratio. The parameters used for the DME reactor are listed in Table 2.

Table 2 Fixed parameters for DME reactor design.

N° tubes	Diamater [m]	Bed voidage	density $Cu/ZnO/Al_2O_3$ [kg/m^3]	density γ-Al_2O_3 [kg/m^3]	ρ average [kg/m^3]	Temperature (^{o}C)	Pressure (bar)
5000	0.02	0.45	1200	1470	1380	250	50

2.2.6 DME distillation unit

The produced DME contains significant impurities, requiring a separation or distillation unit to obtain pure dimethyl ether. The distillation plant comprises a cooling and a gas-liquid separation unit. The cooling unit, represented in the layout by a vapour-liquid separator (VLS), is used to produce chilled streams at -40°C resulting in a liquid stream of DME with dissolved CO_2 and MeOH (stream 17) and a gas stream of incondensable gases, namely, H_2, CO, undissolved CO_2 and traces of other diluents (steam 47). The gas stream is re-circulated into the oxyfuel unit and burnt, while the liquid stream is further processed in the gas-liquid separation unit. The gas separation unit is composed of three different distillation columns: CLN-CO_2, CLN-DME, and CLN-MEOH (Table 3). The first one is used to separate the dissolved CO_2, the second to produce a pure 99% DME and the last one to separate the methanol from the water. Thus, an additional fuel as methanol is

generated as a by-product of DME distillation. A valve and a heat exchanger are placed before each column in order to adjust the pressure to the optimal value and to have 50% of vapor in the inlet stream [71]. The number of stages used in the distillation columns was estimated by increasing them until a certain change in composition was detected.

Table 3 Distillation unit operation parameters.

Column	T_{REB} [°C]	Q_{REB} [MW]	T_{cond} [°C]	Q_{cond} [MW]	Number of stages	Feed-in stage	Purity of the product [%]
CLN-CO_2	45.87	1.12	-40.83	-0.64	25	10	-
CLN-DME	150.99	0.93	42.57	-0.55	30	24	99.1
CLN-MeOH	101.53	0.03	66.36	-0.05	24	18	94.1

3. Synthesis of DME

3.1 Reaction scheme

DME production can be realized in two steps (methanol and DME are produced in two different reactors) or in a single step adopting a dual catalyst. The disadvantage of the two-step process is that syngas conversion to methanol is significantly limited by equilibrium and thermodynamic constraints [72]. The conversion of methanol to DME in the single step process shifts the equilibrium toward more methanol production. Consequently, the direct DME synthesis is thermodynamically and economically preferable than the two steps process [73–75] and hence selected in the present study. The overall process can be described by three main reactions: the syngas conversion to methanol (reaction (4)), water gas shift (reaction (5)) and methanol dehydration to DME (reaction (6)).

$$CO_2 + 3H_2 \rightarrow CH_3OH + H_2O \quad -\Delta H_{298\ K;0.1\ MPa} = 49.2\ kJ/mol \tag{4}$$

$$CO + H_2O \rightarrow CO_2 + H_2 \quad -\Delta H_{298\ K;0.1\ MPa} = 41.2\ kJ/mol \tag{5}$$

$$2CH_3OH \rightarrow CH_3OCH_3 + H_2O \quad -\Delta H_{298\ K;0.1\ MPa} = 24.0\ kJ/mol \tag{6}$$

The overall reaction to synthesize the syngas to DME route is represented by the combination of reactions (4), (5) and (6) into reaction (7):

$$3H_2 + 3CO \rightarrow CH_3OCH_3 + CO_2 \quad -\Delta H_{298\ K;0.1\ MPa} = 246.0\ kJ/mol \tag{7}$$

The overall reaction is exothermic and generates two molecules of products from six molecules of reactants. Hence, according to the Le Châtelier principle [76], conversion is favored working at high pressure and low temperature.

3.2 Reaction kinetics

The DME reactor was simulated in Aspen Plus with an RPLUG reactor combined with a Langmuir-Hinshelwood Hougen-Watson (LHHW) kinetic model based on three simultaneous reactions (Eqs.4,5,6). Bi-functional catalyst Cu/ZnO/Al_2O_3:γ-Al_2O_3 with a loading ratio of 1:2 has been selected from the literature, with the Cu/ZnO/Al_2O_3 active for the methanol synthesis, while

the γ-Al_2O_3 component catalyzes the methanol dehydration [72] among the other presented in the literature the selected is most investigated [77]. The details of the catalyst properties are reported in Table 2. The kinetic model adopted in the present simulations has been extensive used in the literature [14,71,78–80]. The rate expression for CO_2 hydrogenation, RWGS, methanol dehydration is given by equations (8-10) [72,81,82].

$$r_{CO_2\ hydrogenation} = \frac{k_1\left(p_{H_2}\cdot p_{CO_2}\right)\left[1-\left(\frac{1}{K_{eq,1}}\right)\frac{p_{CH_3OH}\cdot p_{H_2O}}{p_{CO_2}\,p_{H_2}^3}\right]}{\left(1+k_2\frac{p_{H_2O}}{p_{H_2}}+\sqrt{k_3\cdot p_{H_2}}+k_4\cdot p_{H_2O}\right)^3} \quad (8)$$

$$r_{RWGS} = \frac{k_5\cdot p_{CO_2}\left[1-\frac{1}{K_{eq,2}}\frac{p_{CO}\cdot p_{H_2O}}{p_{CO_2}\cdot p_{H_2}}\right]}{1+k_2\frac{p_{H_2O}}{p_{H_2}}+\sqrt{k_3\cdot p_{H_2}}+k_4\cdot p_{H_2O}} \quad (9)$$

$$r_{MeOH\ dehydration} = \frac{k_6\cdot K_{CH_3OH}^2\left[[\Pi]_{CH_3OH}^2-\left(\Pi_{H_2O}\cdot\frac{\Pi_{DME}}{K_{eq,3}}\right)\right]}{\left(1+2\sqrt{K_{CH_3OH}\cdot\Pi_{CH_3OH}}+K_{H_2O}\cdot\Pi_{H_2O}\right)^4} \quad (10)$$

Reaction rates of equation (8-10) are expressed in kmol/kg_{cat} s, p is the partial pressure of the gases in Pa and Π the concentration expressed in kmol/m^3. The equilibrium constant (K_i) and constant rate (k_i) values used to determine the reaction rates are shown in Table 4.

Table 4. Kinetic parameters used in DME synthesis.

	Pre	unit	B	unit
k_1	1.07×10^{-13}	(kmol/(kg-sPa^2))	36,696	(J/mol)
k_2	3450	-	0	(J/mol)
$k_3^{0.5}$	1.578×10^{-3}	$Pa^{-0.5}$	17,197	(J/mol)
k_4	6.62×10^{-16}	Pa^{-1}	124,119	(J/mol)
k_5	122	(kmol/(kg s Pa))	-94,765	(J/mol)
k_6	1.486×10^{11}	(kmol/(kg s))	-143,666	(J/mol)
K_{CH3OH}	5.39×10^{-4}	m^3/kmol	70,560.92	(J/mol)
K_{H2O}	8.47×10^{-2}	m^3/kmol	42,151.98	(J/mol)

These parameters refer to the Arrhenius equation shown by equation (11).

$$k_i = (\mathrm{Pre})_i \times \exp\left(\frac{B_i}{RT}\right) \quad (11)$$

where B represents either the activation energy or the reaction enthalpy or a combination of both [81] as in LHHW kinetic mechanism the rate constants are represented as combination of rate constants and equilibrium constants. The following expressions were used to determine the equilibrium constants [55,81,83].

$$\log_{10} K_{eq,1} = \frac{3066}{T} - 10.592 \quad (12)$$

$$\log_{10}(1/K_{eq_2}) = -\frac{2073}{T} + 2.029 \quad (13)$$

$$\ln K_{eq,3} = \frac{3220}{T} - 1.7 \quad (14)$$

The model was used to perform a sensitivity analysis of methanol and DME yield using the equations (15) and (16) varying the composition of the inlet stream, H_2:CO ratio, and the amount of the diluent H_2O and CO_2.

$$DME_{yield} = \frac{DME_{out}}{(CO + CO_2)_{in}} \quad (15)$$

$$MeOH_{yield} = \frac{MeOH_{out}}{(CO + CO_2)_{in}} \quad (16)$$

Where DME_{out} and $MeOH_{out}$ are the DME and methanol molar flow at the outlet of the reactor (stream 15) and CO and CO_2 the molar flow at the inlet (stream 14).

As shown in Figure 5 the highest DME yield is obtained by feeding a syngas with an H_2/CO =1 with a positive effect of having the main byproduct of the reaction as CO_2 which can be easily separated from the DME and MeOH in the separation unit which is verified from the results reported by Ogawa et al [41] . At H_2/CO=1, the DME yield was 38.6% and MeOH yield was 0.8% which are similar to the results reported by Pozzo et al [71]. It is observed that with increasing the CO_2 content at the inlet feed, the DME yield decreases. This is attributed mainly to two factors. Firstly, the methanol synthesis is retarded with the increase of CO_2 content [84] as CO_2 molecules are absorbed by the methanol catalyst by occupying the active sites quicker than CO and H_2, affecting the MeOH production and consequently also the DME synthesis [85] as shown in Figure 6(a). Secondly, with a high CO_2 concentration in the feed of the DME reactor, the beneficial effect of the water gas shift reaction would get decreased. The water formed is removed by WGS producing hydrogen which kinetically advances the methanol production. Therefore, the higher CO_2 favors the reverse-water gas shift that reduces the hydrogen content and produces more water. The effect of higher water content at the inlet is even worse than CO_2 and it can be seen in Figure 6(b). The high water percentage shifts the methanol dehydration towards the reactants, increasing the

MeOH yield while reducing the DME yield. With a water percentage higher than 20%, also methanol production is penalized. In addition, the water tends to deposit near the catalyst accelerating the catalyst degradation [41]. Therefore, to increase the DME production it is necessary to have at the inlet of the DME reactor a syngas composed by an equimolar H_2-CO mixture, reduce the CO_2 percentage (molar fraction) in the 0-5% range and remove as much as possible the water content.

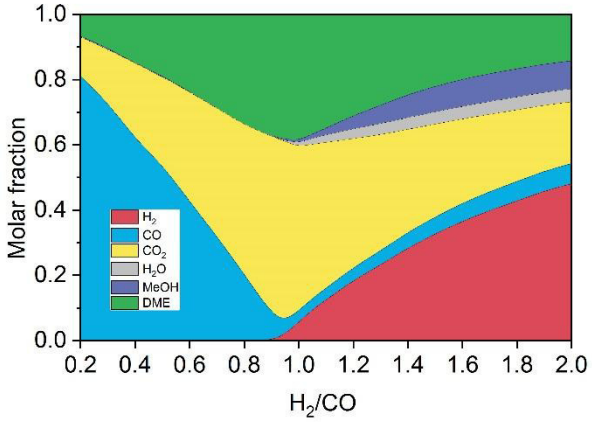

Figure 5: Influence of the H_2/CO ratio on the equilibrium synthesis of DME at T=250°C and p=50 bar.

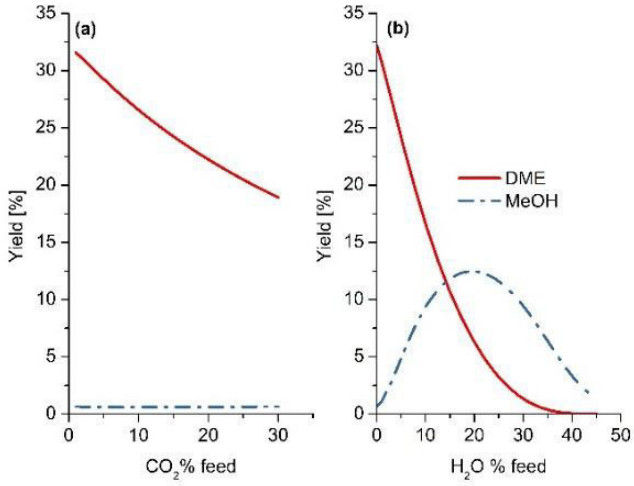

Figure 6: a) Influence of the CO_2 and b) H_2O on the equilibrium synthesis of DME at T=250°C and p=50 bar.

4. Results

4.1 Effect of operating conditions

A sensitivity analysis of the most influential parameters – namely: the operating pressure of the chemical looping CO_2/H_2O splitting unit, outlet temperature of reduction reactor, CO_2/H_2O composition in the oxidation reactor of the CL unit, and turbine inlet temperature – was performed to maximize the global efficiency of the plant (Eq. 17) and the DME production.

$$\eta_c = \frac{\dot{m}_{DME} \cdot LHV_{DME} + \dot{m}_{MEOH} \cdot LHV_{MEOH} + W_{NET}}{\dot{m}_{NG} \cdot LHV_{NG}} \quad (17)$$

where: $\dot{m}_{DME}$, $\dot{m}_{MeOH}$ represent the DME and MeOH streams produced (kg/s), while LHV_{DME}, $LHV_{MeOH,}$ and LHV_{NG} are the lower heating value (MJ/kg) of DME, MeOH and natural gas respectively, and W_{NET} is the net power (MW) produced inside the plant with $\dot{m}_{NG}$ being the natural gas stream feed into the plant (kg/s).

4.1.1 Chemical looping (CO_2/H_2O) splitting (CL) unit pressure

Figure 7 shows the effect of varying the pressure of the chemical looping unit, where both oxidation and reduction reactors work at the same pressure. With the increase of pressure of the CL unit, an efficiency gain is observed from 49.4% at 1 bar to 51.1% at 5 bar. This can be attributed to the fact that a significant saving of the auxiliary power compression ($W_{COMP,tot}$ in Figure 7) is obtained by reducing the pressure ratio of syngas compression. However, with a further increment of the pressure, the efficiency decreases, dropping down to 43.6% with 20 bar of pressure. Based on the Le Châtelier principle, it can be understood that the reaction in the RED reactor is not thermodynamically favored at high pressure since the reduction reaction has three moles of reactants and four moles of products. In fact, it can be seen that over 5 bar the amount of reduced ceria (Ce_2O_3 line in Figure 7) at the outlet of the reactor decreases. This results in a lower syngas production from the OXI reactor, as less reduced ceria is available, subsequently, the DME production drops effecting the overall plant efficiency. DME production drops after 5 bar pressure and it does not vary between 1 to 5 bar while the W_{NET} increases very slowly from 100 to 105 MW. The CL unit pressure can be fixed to 2 bar as the benefit of working at higher pressure is offset by the power required to maintain pressure drop while working with solids.

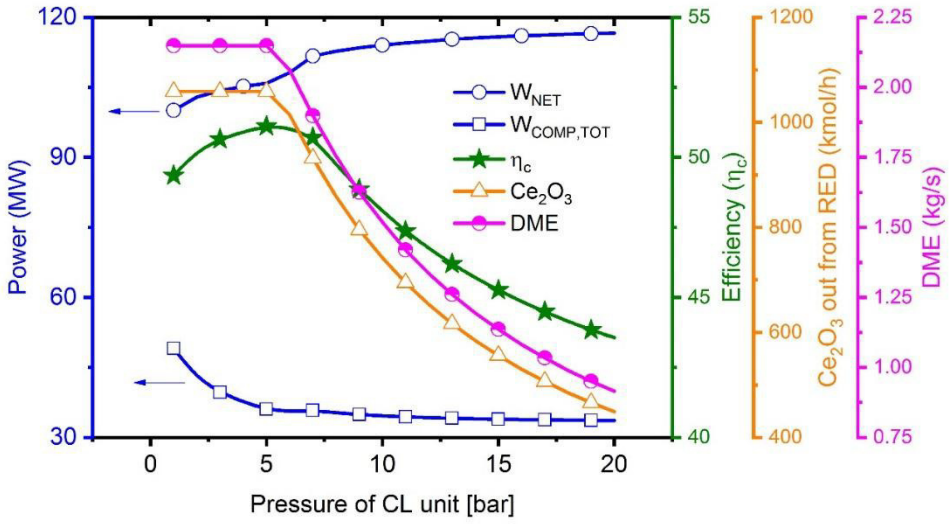

Figure 7 Influence of chemical looping unit pressure on efficiency η_c, W_{NET}, Ce_2O_3 outlet from RED and $W_{COMP,tot}$ ($=W_{COMP-1}+ W_{COMP-2}+ W_{COMP-3}$).

4.1.2 Outlet temperature of the RED reactor

Another fundamental parameter is the outlet temperature of the OC from the RED. It is found that below 900°C there is no complete metal oxide conversion, similar to the results observed by Warren and Scheffe [31]. Therefore, all the analysis were performed considering reduction temperature above 900°C. A higher OC temperature at the outlet of the reactor, inherently demands

more heat supply. Since this heat is derived from the heat of combustion, to have higher RED temperature, less CO_2 needs to be recirculated to the combustion chamber. This, even though results in a corresponding drop in the power spent for recycling CO_2, also implies a lower mass flow through the GT, producing less power, as shown in Figure 8. Such would then lower the power produced by the ST1 as well, notwithstanding the higher temperature of the GT outlet, and hence decreasing the net power output. In addition, a higher outlet temperature of RED also restricts the effective operation of the OXI. In fact, since both the CO_2 and H_2O splitting reactions are exothermic, by principle, this requires the reactions to take place at a lower temperature. Moreover, the water-splitting reaction has a higher exothermicity than CO_2 splitting with Ce_2O_3; thus, a higher temperature would result in a slower reaction rate for H_2O splitting, resulting in a CO-rich syngas. This effect is evident in Figure 8, in which a significant drop in the DME production can be seen beyond 1000°C (from 2.15 kg/s for 900°C to 2.13 kg/s at 1000°C and to 1.99 kg/s at 1100°C) due to a deviation from the ideal H_2-CO ratio and higher concentration of CO_2 in the produced syngas stream (Figure 9).

DME is one of the primary products of the proposed polygeneration system, a decrease in the DME production has a dramatic impact on the plant efficiency, as clearly observed in Figure 8 where the drop in the DME yield drives the trend of the decrease in the overall plant efficiency. To be more specific, a relative drop of 10.5% in efficiency is observed between 1000°C and 1300°C, corresponding to an in DME production of 24% and a relative net power output drop of 2%.

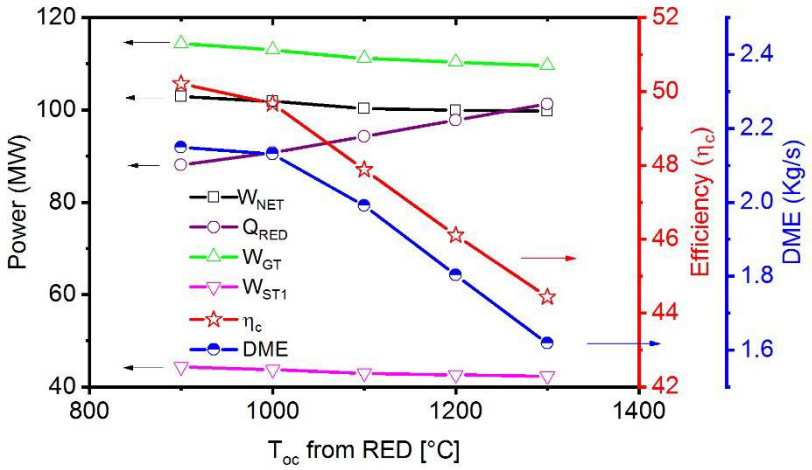

Figure 8 Influence of the metal oxide outlet temperature of RED on efficiency (η_c), W_{NET}, W_{ST1}, W_{GT} Q_{RED} , and DME production

Figure 9 shows the effect of the metal oxide inlet temperature to the OXI on the H_2/CO ratio in the syngas and on the CO_2 content in the syngas after water removal. As mentioned before, water splitting is favored at a lower temperature compared to CO_2 splitting due to the higher exothermicity of the reaction. Hence, in order to have the ideal H_2/CO =1 for DME production, it is necessary to send an increasingly H_2O rich mixture with the higher temperature to the OXI. In fact, with the increase of the OC temperature, the water splitting is further penalized and consequently, a higher H_2O content ranging from 60% to 74% for OC temperature from 900-1300°C. In addition, as already explained in section 2.2.5, the dilution of syngas with CO_2 has to be avoided in order to enhance DME production. As shown in Figure 9(b), even if it might be possible to produce the ideal composition of syngas (i.e., 1:1 H_2/CO ratio) for any metal oxide temperature inlet, the CO_2 content

increases at higher temperatures. For this reason, it is suitable to work with lower ceria inlet temperature (900-1000°C) to avoid CO_2 dilution.

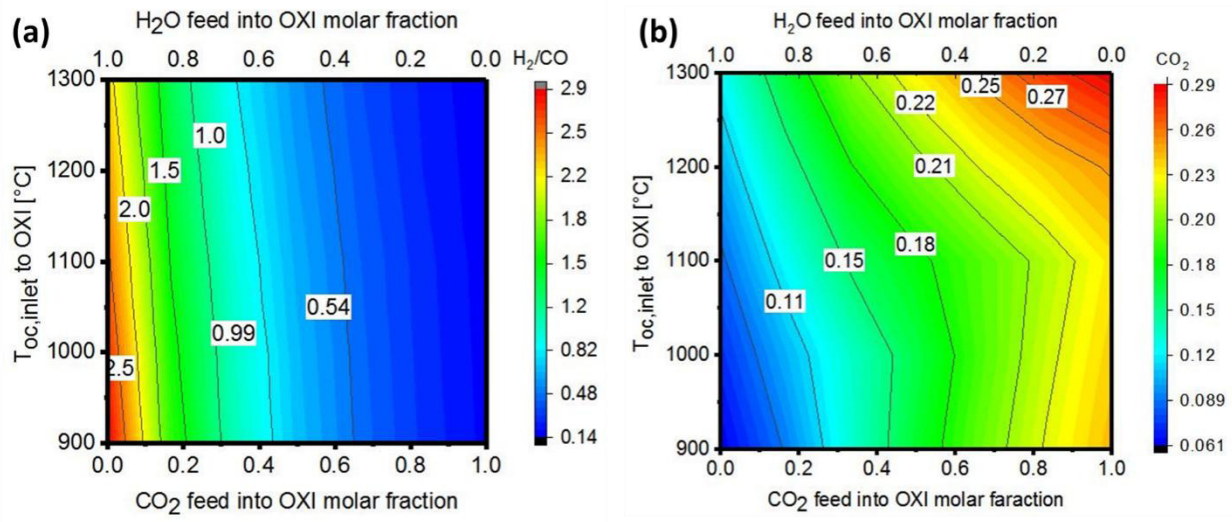

Figure 9 Effect of the gas mixture composition fed into OXI on a) final syngas H_2/CO ratio, b) CO_2 content (molar fraction) in the syngas after water removal.

4.1.3 Composition of inlet gas mixture to the OXI

Figure 10 describes the effect of the variation of the gas mixture composition at the inlet of the OXI on plant performance. The maximum efficiency of 50% is achieved with an OXI inlet mixture of 60% of H_2O and 40% CO_2. In such a condition, the OXI outlet gas has the equimolar H_2:CO ratio (i.e., H_2 and CO curves intersect) which reflects the maximum DME production. Similar claims has been presented by Ohno et al [86].

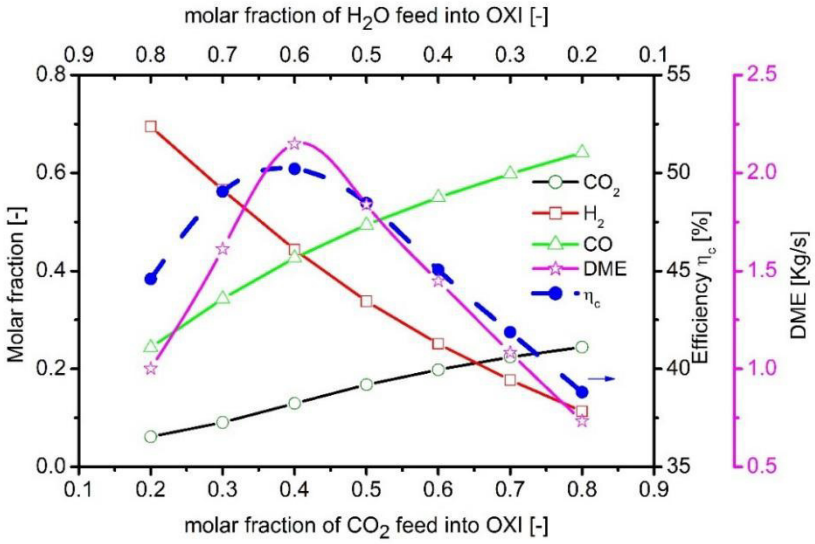

Figure10 Influence of the gas mixture composition at the inlet of the OXI reactor on the plant performance by considering a metal oxide outlet temperature from the RED equal to 900°C.

Increasing the water content in the feed to OXI reactor increases outlet metal oxide temperature (Figure 11(a)) as water splitting is more exothermic than CO_2 splitting reaction. In the proposed

OXYF-CL-PFG plant layout, the oxidized ceria is recirculated back to the reduction reactor without intermediate heat recuperation. Hence, a higher temperature of oxidized ceria at the outlet of OXI results in a higher inlet temperature of OC to the RED which thereby reduces the heat requirement for the reduction reaction. Due to inlet higher temperature of OC to the RED reactor, the heat requirement from the combustion chamber reduces and therefore, the recirculation of CO_2 to the combustion chamber to maintain the temperature of the outlet would be increased. With this, the power output from the gas turbine (GT) increases as higher flow expands which increases the net power production, as seen in Figure 11(d). As stated earlier, this can be possible with the higher H_2O concentration in the feed of OXI which increases the H_2/CO ratio more than unity leading to the drop in DME production and overall efficiency (see Figure 11(b) and (c)). Therefore, an ideal H_2/CO ratio feed to DME reactor, even though leads to lower overall net power, however, ensures the highest efficiency of the polygeneration unit, as can be understood from Figure 11(d). In the case of a non-ideal H_2/CO ratio being fed to the DME reactor, it leads to a lower conversion with unreacted syngas in the product stream. Even though after distillation, this is recycled to the combustor increasing the power, but reduces the DME production and thus, the overall efficiency of the plant.

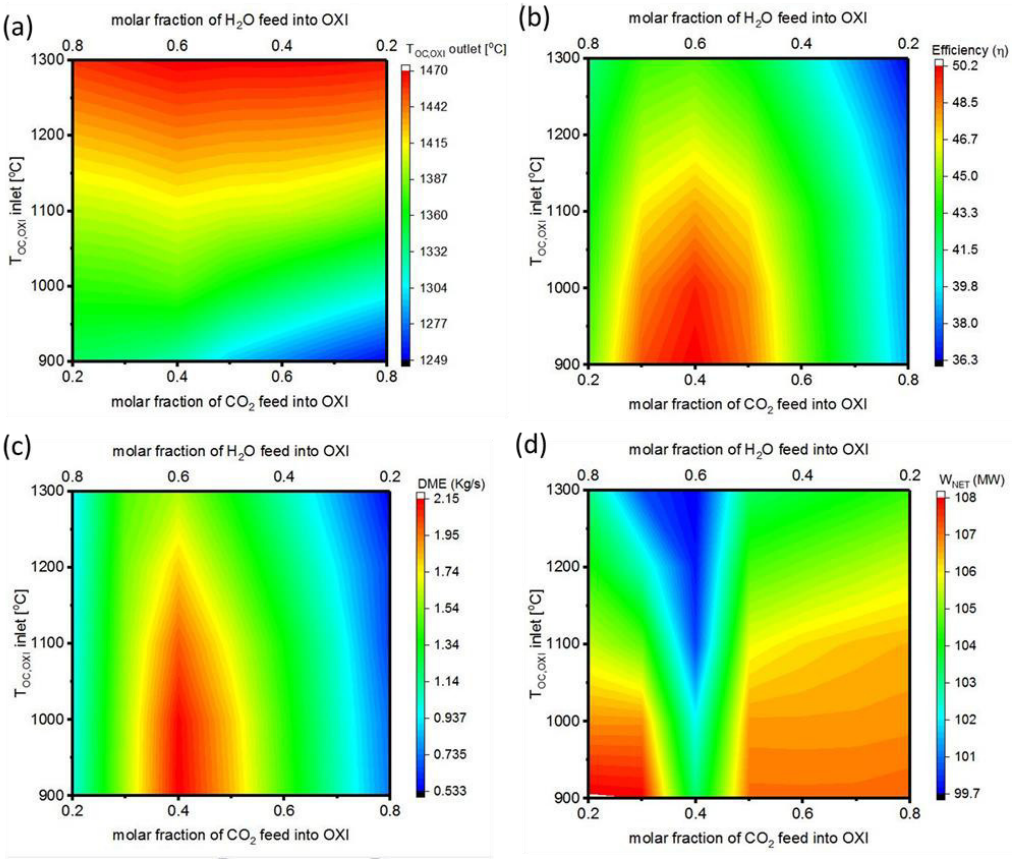

Figure 11 Effect of the gas mixture inlet composition and metal oxide inlet temperature ($T_{OC,OXI}$ inlet) on (a) the temperature of the metal oxide outlet, (b) plant efficiency, (c) DME production, and (d) net power.

4.1.4 Gas turbine inlet temperature

Finally, the impact of the gas turbine inlet temperature (TIT) was analyzed. It can be said from Figure 12 that with an increase of TIT the efficiency and net power produced are positively influenced. Nevertheless, the output from the GT drops, which is the result of a lower recirculation

of CO_2 to the combustor, needed to ensure a higher combustor exit temperature and consequently a higher TIT. This also causes a lower gas volume to be expanded within the GT, resulting in a lower power output, even though a partial compensation of the lost work is obtained by the lower compression work for the recirculated CO_2 in COMP-2. The power produced by the steam turbine ST1 increases slightly due to a higher exhaust temperature from the GT, overcoming the lower overall gas flow rate. For a TIT of 1100°C, the efficiency of 47.6% was obtained, which increases to 50.7% for a TIT of 1450°C.

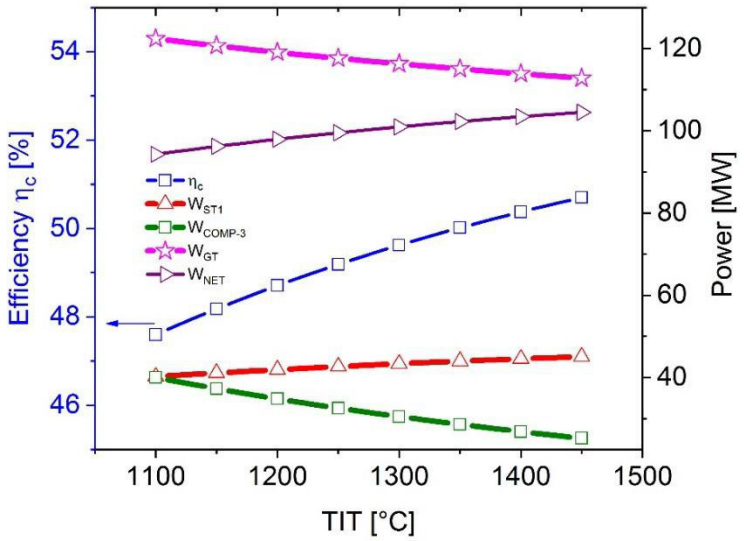

Figure 12 Effect of the gas turbine inlet temperature TIT on the efficiency of the plant (η), power produced by the steam turbine (W_{ST1}), by the gas turbine GT (W_{GT}) and the power absorbed by the COMP-3 (WCOMP-3)

4.2 Plant performance

Based on the sensitivity analysis the following operating parameters were chosen:

- chemical looping operation pressure of 2 bar;
- 40% CO_2 and 60% H_2O in the gas mixture feed to the oxidation reactor with an excess of 60% with respect to the stoichiometry as per the Ce_2O_3 inlet to OXI;
- reduction reactor outlet temperature 900°C;
- TIT of 1377°C.

The plant performance based on the listed parameters is summarized in Table 5. Overall, the plant produces 102.90 MW_e, 185.6 ton/day (2.15 kg/s) of DME and 2.59 ton/day (0.03 kg/s) of methanol with a total efficiency of 50.21% and a DME yield of 24.9% (as per equation (8)). The highest power consumption is represented by the COMP-3 for the recycle of the CO_2 followed by the compression work in the ASU which accounts for 17% and 11.5% of the gross power generated respectively. Table 6 lists the composition and main thermodynamics parameters of major streams.

The inlet stream to the DME reactor (stream 14) has the ideal H_2/CO =1 ratio, while the CO_2 content is 13%. However, it can be seen in Figure 11(b), that the minimum CO_2 percentage which can be achieved from the oxidation reactor is near 6%, even though not producing the equimolar mixture of H_2/CO. Therefore, the actual plant configuration allows producing a syngas with a composition which diverges from the ideal H_2/CO ratio of syngas. A solution might be to propose

two distinct oxidation reactors, one for the CO_2 splitting and another for the water-splitting. However, this will lead to two different oxidized metal oxide temperatures, complicating the system design dynamics and operations.

An encouraging result is that the proposed oxyfuel-NGCC cycle with the chemical looping and DME unit permits to cut the efficiency penalty of CCS. In particular, compared with results from literature [87], it is possible to achieve a gain of 4 percentage points with respect to a stand-alone Oxyfuel-NGCC process[1].

To evaluate the overall plant performance with regards to CO_2 savings, besides calculating the overall CO_2 avoided, the plant carbon efficiency, C_{eff} provides an alternative measure as per the following equation (18) [78,88,89].

$$C_{eff} = \frac{\dot{m}_{C,DME} + \dot{m}_{C,MeOH}}{\dot{m}_{C,NG}}, \quad (18)$$

where $\dot{m}_{C,DME}$ and $\dot{m}_{C,NG}$ are respectively the mass flow of carbon contained in the product (DME) and the primary reactant (inlet NG stream) respectively. $\dot{m}_{C,MeOH}$, denoting the mass flow of carbon in methanol contributes an minor fraction to the overall carbon efficiency of the polygeneration system as well.

The total CO_2 produced in polygeneration plant is 3.36 million tons per year out of which 3.4% is converted to the DME ($CO_{2,DME}$) with an overall plant carbon efficiency of 22.25% (Table7). The recirculation streams of CO_2 ($CO_{2,REC}$) in the combustor accounts for the 85% produced CO_2 from the exhaust (2.86 million tons per year), while the one sent into OXI for dissociation is 6.54%. In addition, a polygeneration scheme ensures the ability to produce DME within the same system, thus cutting emissions from stand-alone DME production. Conventional DME production via a stand-alone steam methane reforming process results in an equivalent CO_2 emission of 51.1 $kgCO_2/GJ$ of DME [53]. Therefore, an equivalent of an additional 85.65 kilotonne of CO_2 was saved by the polygeneration scheme accounting of total 589.15 kilotonne of CO_2 avoided annually. More detailed share of carbon capture and utilization is listed in table S2 in supplementary file. As for the carbon efficiency, the CL unit pressure and increase in CO_2 content to the OXI form the most negative impacts, as can be observed from Table 7. This can be concluded from the decrease in DME production, indicating the contribution of different operating conditions to the overall optimal operation of the polygeneration plant.

Table 5 Plant results with selected parameters.

NG feed	25.2 ton/h
W_{GROSS}	167.61 MW
W_{NET}	102.90 MW
η_c	50.21%
W_{COMP-1}	3.76 MW
W_{COMP-2}	10.67 MW

[1] considering 0.09 kWh/Nm^3 energy requirement for CO_2 compression [113].

W_{COMP-3}	28.29 MW
W_{ASU}	19.34 MW
W_{GT}	114.42 MW
W_{ST1}	44.30 MW
W_{ST2}	2.96 MW
$W_{TURBEXP}$	4.37 MW
$\dot{m}_{DME}$	185.6 ton/day (2.15 kg/s)
$\dot{m}_{MeOH}$	2.59 ton/day (0.03 kg/s)
$CO_{2,REC}$	85%
$CO_{2,DME}$	3.4%

Table 6. Thermodynamics properties and composition of selected streams.

Stream	28	10	14	15	17	20	31	37	38	43	47	7	9
T (°C)	900	1322	200	250	46	43	1377	80	40	40	-41	900	1322
P (bar)	2	2	5	50	10	9	26	26	1	1	10	2	2
Mole flow (kmol/s)	1	0.47	0.34	0.15	0.05	0.04	3.67	2.44	0.19	0.28	0.09	0.59	0.29
Molar fraction													
H_2	0.57	0.32	0.44	0.04	0	0	0	0	0	0	0.01	0	0
H_2O	0	0.28	0	0.01	0.03	0	0.22	0	0	0.99	0	0	0
CO_2	0	0.09	0.13	0.6	0	0	0.77	0.99	0.99	0	0.96	0	0
CO	0.29	0.30	0.43	0.03	0	0	0	0.01	0	0	0.03	0	0
CH_4	0.12	0	0	0	0	0	0	0	0	0	0	0	0
other gases*	0.02	0.01	0	0	0	0	0	0	0.005	0.01	0	0	0
MeOH	0	0	0	0.01	0.02	0.01	0	0	0	0	0	0	0
DME	0	0	0	0.31	0.95	0.99	0	0	0	0	0	0	0
CeO_2	0	0	0	0	0	0	0	0	0	0	0	1	0
Ce_2O_3	0	0	0	0	0	0	0	0	0	0	0	0	1

*other gases include N_2 and other trace gases of natural gas

Table 7. Overall plant carbon efficiency for specific plant operating parameters.

Plant Operation Conditions	CL Unit Pressure [bar]	Toc from RED [°C]	H_2O%:CO_2% feed to OXI	Gas Turbine TIT [°C]	Carbon Efficiency (*Ceff*) [%]
Ideal	2	900	40:60	1377	22.25%
High CL Unit Pressure	20	900	40:60	1377	9.48%
High Toc from RED	2	1300	40:60	1377	16.70%
High CO_2 % in OXI gas Feed	2	900	80:20	1377	7.60%
High H_2O % in OXI gas Feed	2	900	20:80	1377	10.40%
High Gas Turbine TIT	2	900	40:60	1450	22.25%

5. Pinch analysis

The thermal integration of the proposed polygeneration plant was performed using the pinch point analysis [90]. The highest temperature of 1322°C corresponds to the oxidation reactor outlet,

while the lowest of -40°C is the DME condensation temperature. Figure 13 shows the hot and cold composite curve indicating a good thermal integration between cold and hot utilities, without the use of an external heat source. Therefore, the scope for a further increment in the efficiency of the power plant through optimized heat integration is limited. Starting from the hotter utilities, the profile can be interpreted as follow:

- The cold utility curve from 50°C to 550°C represents the steam generation (stream 2A-5A and 2B-5B) driven by the exhaust gas from GT (stream 32) and the hot syngas from the oxidation (stream 10). It also represents the CO_2-H_2O preheating before the dissociation (stream 39 and 45) driven by stream 10a and 10b (hot syngas) in the HX-5 and HX-10 (for CO_2 preheating) and HX-4 and HX-12 (for H_2O preheating);
- The steep part of the curves, from 550° to 900°C for the cold utilities, represents the of natural gas preheating before the reduction in RED (stream 5) taking place in the heat exchangers (HX-1 and HX-8B) and (HX-2 and HX-8);
- The part of the curves near and below zero is mostly related to the distillation unit and the condensation up to a temperature of -40°C of the DME;

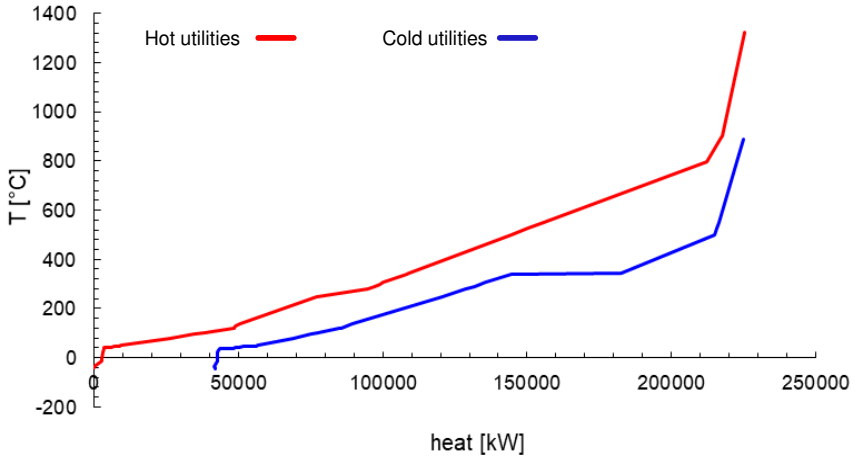

Figure 13 Pinch point analysis with hot and cold composite curves

6. Exergy analysis

Exergy of a steady stream of matter is defined as the maximum amount of work obtainable when the stream is brought from its initial state to the dead state by processing during which the stream may interact only with the environment [91]. Exergy (E) can be divided into different components: kinetic exergy E_k, potential exergy E_{pot}, physical exergy E_{ph} and chemical exergy E_{ch}.

$$E = E_k + E_{pot} + E_{ph} + E_{ch} \quad (19)$$

In the presented exergy analysis, the physical and chemical exergy are considered. The physical exergy is defined as the maximum work achievable from a system that from its initial state is

brought to the environmental state with only thermal and mechanical interaction with the environment. While the chemical exergy is the maximum work obtainable from a system that is brought from the environmental state to the dead state involving heat transfer and exchange of substances only with the environment. The two types of exergy are given by equation (20) and (21)[92]. In particular, for a mixture, the total chemical exergy $E_{ch,tot}$ is made by two contributes: the chemical exergy of the single i-th component $E_{0,i}$ and the work obtainable from a reversible isothermal expansion at T_0 from the partial pressure p_{00} of the i-th component and environment pressure $p_{0.}$

$$E_{ph} = \sum_i x_i \cdot \left[\left(h_i - h_{0,i} \right) - T_0 \cdot \left(s_i - s_{0,i} \right) \right] \quad (20)$$

$$E_{ch,tot} = \sum_i x_i \cdot \left[E_{0,i} + \varphi \cdot R \cdot T_0 \ln \frac{p_0}{p_{00}} \right] \quad (21)$$

The exergy analysis is based on the second principle of thermodynamics, thus permits to evaluate the so-called ‘‘destroyed’’ exergy ($I_{destroyed.}$). Destroyed exergy represents the real loss in the quality of energy that cannot be identified by means of a simple energy balance because the conservation of energy will always apply. The following equation represents an exergy balance of a general device in steady state condition:

$$\sum_i (E_{out,i} - E_{in,i}) = \sum_i W_i + \sum_i Q_i \left(1 - \frac{T_0}{T_i} \right) + I_{destroyed} \quad (21)$$

In equation (21): i) the members at the left side represent the exergy contribution of the $E_{in,i}$ inlet and $E_{out,i}$ outlet mass flows, ii) W_i represents the absorbed/produced work by the device, iii) the second member at the right side is the contribution from the heat exchanged, which represents the work obtainable from the heat flux Q_i operating with a Carnot machine, and iv) $I_{destroyed}$ is the irreversibility generated.

In order to estimate the exergy efficiency (or efficiency of the second principle) of a system is necessary to define the resource exergy flow of the process (Fuel) and product of the process (Product). The exergy efficiency is shown by the following equation:

$$\eta_{ex} = \frac{E_P}{E_F} \quad (23)$$

Where E_P represents the exergy of the product streams and E_F the exergy of the resource streams. However, the only exergy efficiency does not give a complete framework of the plant or subsystem. For this reason, an additional exergetic factor and other parameters were adopted [93]:

– Relative irreversibilities: $\chi_i = \frac{I_{i,destroyed}}{I_{tot,destroyed}}$ (24)

– Fuel depletion rate: $\theta_i = \frac{I_{i,destroyed}}{E_{F,plant}}$ (25)

– Productivity lack: $\xi_i = \frac{I_{i,destroyed}}{E_{P,plant}}$ (26)

- Exergetic factor: $\psi_i = \frac{E_{F,i}}{E_{F,plant}}$ (27)

A reference state was selected for the analysis (Table 8). For the environmental state, a pressure (P_0) of 1 atm and a temperature (T_0) of 20°C were selected, while for the dead state the reference environment of Szargut [94] was chosen.

Table 8 Environment state and dead state data of chemical exergy.

Environmental state: P_0=1 atm T_0=20°C											
Dead State											
Chemical exergy E_{ch} (kJ/mol)											
H_2	CO	CO_2	H_2O_{vap}	H_2O_{liq}	N_2	CH_4	O_2	CeO_2	Ce_2O_3 [12]	DME[42]	MeOH[42]
236.09	275.1	19.20	9.181	0.87	0.696	853.36	3.837	33.8	384.7	1414.5	715.52

Since in the proposed layout there are several chemical reactions, which change the composition of the gaseous streams, the first step was to evaluate the reference chemical exergy of the multiple mixture streams using the dead state of the reference elements. The results are shown in Table 9.

Table 9. Specific chemical exergy of the gas mixture streams.

Stream	31	28	10	15	13	47
$e_{ch,i}$ [kJ/kg]	389	27110	7391	11287	11919	6225

The exergetic performance of the overall plant has been assessed by evaluating its exergetic efficiency (Eq. 28) and the total irreversibility generated (Eq. 29). As can be clearly observed pinch analysis, due to both electricity and heat self-sufficiency of the system, the input fuel, namely natural gas, contributes entirely to the net exergy input to the system (i.e., it is 100% of the total exergy input). The products are the total DME, MeOH and the net power produced by the plant.

$$\eta_{ex} = \frac{\dot{m}_{DME} \cdot E_{DME} + \dot{m}_{MEOH} \cdot E_{MEOH} + W_{NET}}{\dot{m}_{CH_4} \cdot E_{NG}} \quad (28)$$

$$I_{tot,\,destroyed} = \dot{m}_{CH_4} \cdot E_{NG} - \dot{m}_{DME} \cdot E_{DME} - \dot{m}_{MEOH} \cdot E_{MEOH} - W_{NET} \quad (29)$$

As expected, since the exergy efficiency is primarily influenced by to the fuel value of natural gas, DME, MeOH, and the net power produced, the exergy efficiency trend is specular to the

thermodynamic efficiency previously described. The energetic and exergetic efficiency with respect to the pressure of CL unit and metal oxide inlet temperature to reduction reactor and turbine inlet temperature is presented in Figure S1 and effect of the molar composition of CO_2 and H_2O in OXI is presented in Figure S2 in supplementary file. Finally, also a detailed exergy analysis of the components of the layout operating at the conditions described in section 4 was performed. Chemical, physical and total exergy values of all streams are reported in Table S3 in supplementary file.

The global exergy efficiency (η_{ex}) of the plant was obtained as 45.0%, five points lower than the calculated first-law efficiency. The total irreversibilities generated are 202.72 MW with an overall fuel depletion rate (θ) of 53.84%. All the components present an exergetic efficiency over the 80%, with the exception of the ASU (55.9%), the two condensers for the steam cycle (32%) and the CLN-MeOH (77%). However, the contribution of COND-A, COND-B, and ASU to the overall efficiency is marginal since their relative irreversibilities χ_i do not exceed the 3.9% (see Table 10).

The exergy efficiency of the RED+COMB results in 88.1%. Although this value is not extremely low, more than half of the 202.72 MW total irreversibilities are in this component (Figure 14). As shown in Table 10, the RED+COMB exergetic factor ψ results in 231.3%, so the irreversibilities are not due to the efficiency but are mainly proportionally correlated to the high exergy of the inlet streams. In fact, the exergy inlet of the RED+COMB ranks first among the components (870 MW), the second being the turbo-expander inlet (378 MW). Moreover, it is worth mentioning that, with the hypothesis of zero heat losses inside the combustor and reduction reactor, the main contributor to the exergy losses are of the chemical form. In fact, the exergy efficiency of the RED+COMB, considering only the chemical exergy of the inlet and outlet streams, results in 70%. The oxidation reactor is the second-ranked component for the relative irreversibilities parameter (14.4%) even if the exergy efficiency (83.4%) results in to be lower than the one of the RED+COMB. This is due to the lower exergy factor (50.7%).

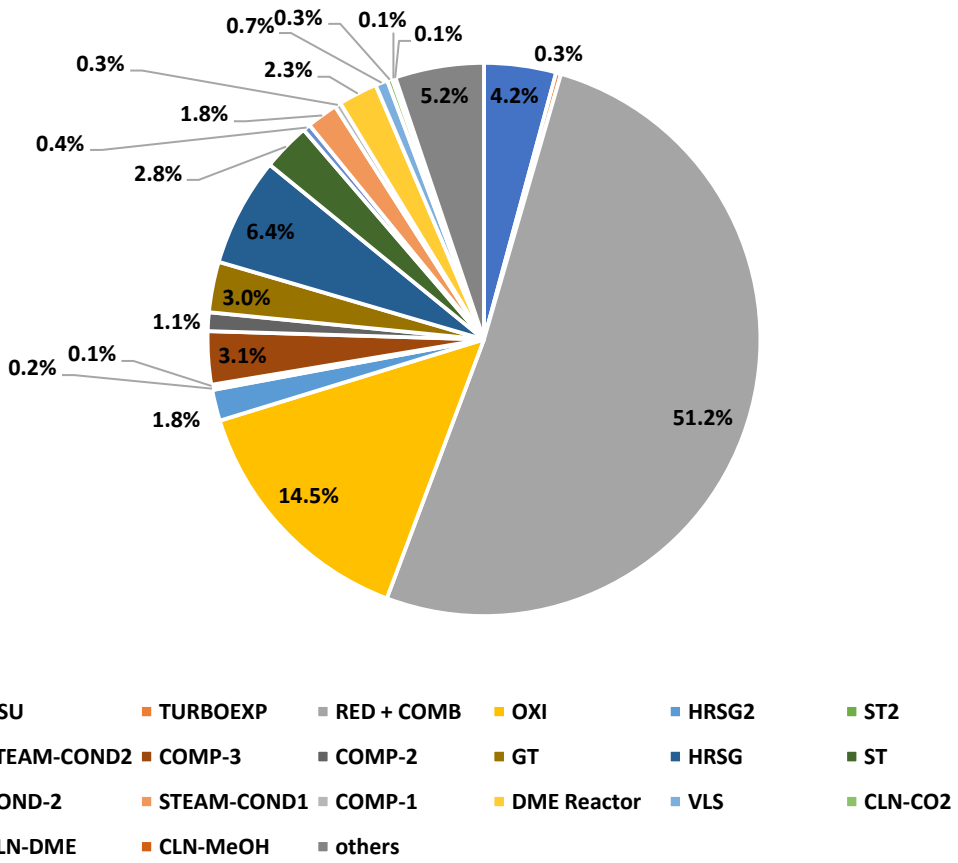

706

707 Figure 5 Total irreversibilities distribution.

708 The other irreversibilities are mostly from the HRSG1 of the steam ranking cycle (SRC1)
709 (13.99 MW) and in the compression process (9.3 MW). The DME reactor jacketing for saturated
710 steam production allows increasing the exergy efficiency of the component of 2.2%.

711 Table 10 Results from the exergetic analysis of the main components.

Componet	Exergy balance eq.[1]	I [MW]	$\eta_{ex,i}$ [%]	θ_i [%]	ψ_i [%]	ξ_i [%]
ASU	$E_0 + W_{ASU} = E_1 + E_{1b} + I_{ASU}$	8.53	55.91	2.26	5.14	5.03
TURBOEXP	$E_3 = W_{TURBOEXP} + I_{TURBOEXP}$	0.59	99.84	0.16	100.41	0.35
RED+COMB	$E_{9a} + E_5 + E_{30} + E_1 + E_{49} + E_{37} = E_{31} + E_{28} + E_7 + I_{RED+COMB}$	103.83	88.08	27.58	231.29	61.23
OXI	$E_7 + E_{46} + E_{40} = E_{10} + E_{9a} + I_{OXI}$	29.47	84.57	7.83	50.74	17.38
HRSG2	$E_{10} + E_{2\text{-}B} = E_{10a} + E_{5\text{-}B} + I_{HSRG\text{-}2}$	3.68	97.49	0.98	38.88	2.17
ST2	$E_{5\text{-}B} = E_{6\text{-}B} + W_{ST2} + I_{ST2}$	0.38	89.77	0.10	0.99	0.22
COND-B	$E_{6\text{-}B} = E_{7\text{-}B} + I_{COND\text{-}B}$	0.25	32.0	0.07	0.10	0.15
COMP-4	$E_{38} + W_{COMP\text{-}4} = E_{39} + I_{COMP\text{-}4}$	0.08	98.26	0.02	1.18	0.04
COMP-3	$E_{49} + W_{COMP\text{-}3} = E_{37} + I_{COMP\text{-}3}$	6.29	91.73	1.67	20.21	3.71
COMP-2	$E_{29} + W_{COMP\text{-}2} = E_{30} + I_{COMP\text{-}2}$	2.21	99.33	0.59	87.57	1.30
GT	$E_{31} = W_{GT} + E_{32} + I_{GT}$	6.00	97.57	1.59	65.57	3.54
HRSG1	$E_{31} + E_{2\text{-}A} = E_{33} + E_{5\text{-}1} + I_{HSRG\text{-}1}$	12.88	90.0	3.42	34.21	7.60
ST1	$E_{5\text{-}A} = E_{6\text{-}A} + W_{ST1} + I_{ST1}$	5.68	89.75	1.51	14.72	3.35
COND-2	$E_{33} = E_{34} + E_{41} + I_{COND\text{-}2}$	0.88	98.51	0.23	15.80	0.52

COND-A	$E_{6\text{-}1} = E_{7\text{-}A} + I_{COND\text{-}A}$	3.71	32.00	0.99	1.45	2.19
COMP-1	$E_{13} + W_{COMP\text{-}1} = E_{14} + I_{COMP\text{-}1}$	0.71	99.10	0.19	20.88	0.42
DME Reactor	$E_{14} + E_{44} = E_{15} + E_{45} + I_{DME\ reactor}$	4.64	94.05	1.23	20.73	2.74
VLS	$E_{15} = E_{47} + E_{17} + I_{VLS}$	1.45	97.99	0.39	19.16	0.86
CLN-CO_2	$E_{19} + Q^{*}_{COND,\ CLN\text{-}CO2} + Q^{*}_{RED,\ CLN\text{-}CO2} = E_{20} + E_{21} + I_{CLN\text{-}CO2}$	0.60	99.15	0.16	18.56	0.35
CLN-DME	$E_{22} + Q^{*}_{COND,CLN\text{-}DME} + Q^{*}_{REB,CLN\text{-}DME} = E_{22} + E_{23} + I_{REB\text{-}DME}$	0.30	99.56	0.08	17.90	0.18
CLN-MeOH	$E_{25} + Q^{*}_{COND,CLN\text{-}MeOH} + Q^{*}_{REB,CLN\text{-}MeOH} = E_{22} + E_{23} + I_{REB\text{-}MeOH}$	0.15	77.39	0.04	0.18	0.09
NG_{PHX1}	$E_2 + E_{28} = E_3 + E_{28b} + I_{NG\text{-}PHX1}$	0.41	99.94	0.11	185.39	0.24
NG_{PHX2}	$E_4 + E_{28b} = E_5 + E_{29} + I_{NG\text{-}PHX2}$	1.59	99.78	0.42	188.17	0.94
CO_{2PHX}	$E_{10a} + E_{39} = E_{10b} + E_{40} + I_{CO2\text{-}PHX}$	0.38	99.48	0.10	19.34	0.23
H_2O_{PHX}	$E_{10b} + E_{45} = E_{11} + E_{46} + I_{H2O\text{-}PHX}$	3.26	95.63	0.87	19.80	1.92

[1]The left-side of the equation in the table represents the fuel of the component, while the right side of the equation represents the product and the irreversibility of the component.
Q^{*} represents the exergy obtainable using the heat of the selected stream

$$Q^{*}_{COND,CLN-CO2}=Q_{COND,CLN-CO2}\times\left(1-\frac{T_{COND,CLN-CO2}}{T_0}\right);$$

$$Q^{*}_{REB,CLN-CO2}=Q_{REB,CLN-CO2}\times\left(1-\frac{T_0}{T_{REB,CLN-CO2}}\right);$$

$$Q^{*}_{COND,CLN-DME}=Q_{COND,CLN-DME}\times\left(1-\frac{T_0}{T_{COND,CLN-DME}}\right);$$

$$Q^{*}_{REB,CLN-DME}=Q_{REB,CLN-DME}\times\left(1-\frac{T_0}{T_{REB,CLN-DME}}\right);$$

$$Q^{*}_{COND,CLN-MeOH}=Q_{COND,CLN-MeOH}\times\left(1-\frac{T_0}{T_{COND,CLN-MeOH}}\right);$$

$$Q^{*}_{REB,CLN-MeOH}=Q_{REB,CLN-MeOH}\times\left(1-\frac{T_0}{T_{REB,CLN-MeOH}}\right);$$

7. Economic analysis

An economic assessment was performed to calculate the capital cost of investment for the construction of the proposed plant. The National Energy Technology Laboratory (NETL) guidelines for techno-economic analysis for power plants was adopted [95,96]. This methodology defines capital cost at five levels: bare erected cost (BEC), engineering, procurement, and construction cost (EPCC), total project cost (TPC), total overnight cost (TOC) and total as-spent cost (TASC). In the current study, the TOC was considered for the capital investment expenditure. The first four items are "overnight cost" and are expressed in base-year US dollar that is the first year of capital expenditure. The Bare Erected Cost (BEC) comprises the cost of the equipment, facilities and infrastructure, and labor required for its installation. The equipment cost was estimated using the scaling factor exponent M, as given by equation (30) [97] and details of which can be found in [12].

$$C_{equ}=C_{equ,ref}\,(J/J_{ref})^{M} \quad (30)$$

where C_{equ} and $C_{equ,ref}$ represent the equipment cost with a capacity of J and J_{ref}, respectively.

To assess further costs related to setting up of the polygeneration plant including installation and other direct and indirect costs related to the project development, a bottom-up approach following the methodology adopted in the CAESER project [98] was selected. All the estimated equipment costs (Table S5 in supplementary file) were converted to the year 2017 US dollar using the chemical engineering plant cost index (CEPCI, Table S6 in supplementary file).

$$C_{equ,actual} = C_{equ,ref} \frac{\text{CEPCI 2017}}{\text{CEPCI at the time of original cost}} \quad (31)$$

The cost of the cooling tower system was included in the cost of the four condensers (COND-1, COND-2, SRC1, and SRC2 condenser). The overall cost was subdivided between the four components proportionally to the calculated rejected heat. The cost of the two condensers (COND-A and COND-B) of the two HRSG were included in the HRSG investment cost. The most expensive equipment is the ASU, followed by the GT. The RED+COMB unit accounts for 5.2% of the total expenditure. The individual contribution of the respective equipment to the total overnight cost is shown in Figure 15.

The bare erected cost (BEC) of each equipment was given summing all the installation costs (see Table S6 in the supplementary file for assumptions of CAPEX estimation) to the equipment cost is given by equation (32).

$$BEC = C_{equ,actual} + \text{Installation Cost} \quad (32)$$

The engineering, procurement and construction cost (EPCC) comprises the BEC plus the costs of all services provided by the engineering, procurement and construction contractor (equation (33)). These items include detailed design, contractor permitting and project management costs.

$$EPCC = BEC + \text{INDIRECT COST} \quad (33)$$

The total project cost (TPC) also includes the contingencies cost (equation (34))to account for unknown costs that are omitted or unheralded due to lack of complete project definition or uncertainties with the development status of a technology. In the present case, since the proposed plant is based on a novel technology arrangement, a high contingency cost of 30% was selected (Table S6 in supplementary file).

$$TPC = EPCC + \text{CONTINGENCIES} \quad (34)$$

The total overnight cost (TOC) comprises the TPC plus other overnight costs (Table S4 in supplementary file), owner's cost included (i.e pre-production, inventory capital, land, financing), it was calculated as:

$$TOC = TPC + \text{OWNER'S COST} \quad (35)$$

From the assumptions listed in Table S6 (in supplementary file), the total overnight cost (TOC) of the plant resulted in 537.45 $million. Figure 15 represents the contribution to the total overnight

cost of the different equipment. The most expensive equipment resulted in the ASU, followed by the GT. The RED+COMB unit accounted for 5.2% of the total expenditure. For the economic analysis, all assumptions are listed in Table S7 and S8 in the supplementary file for OPEX estimations.

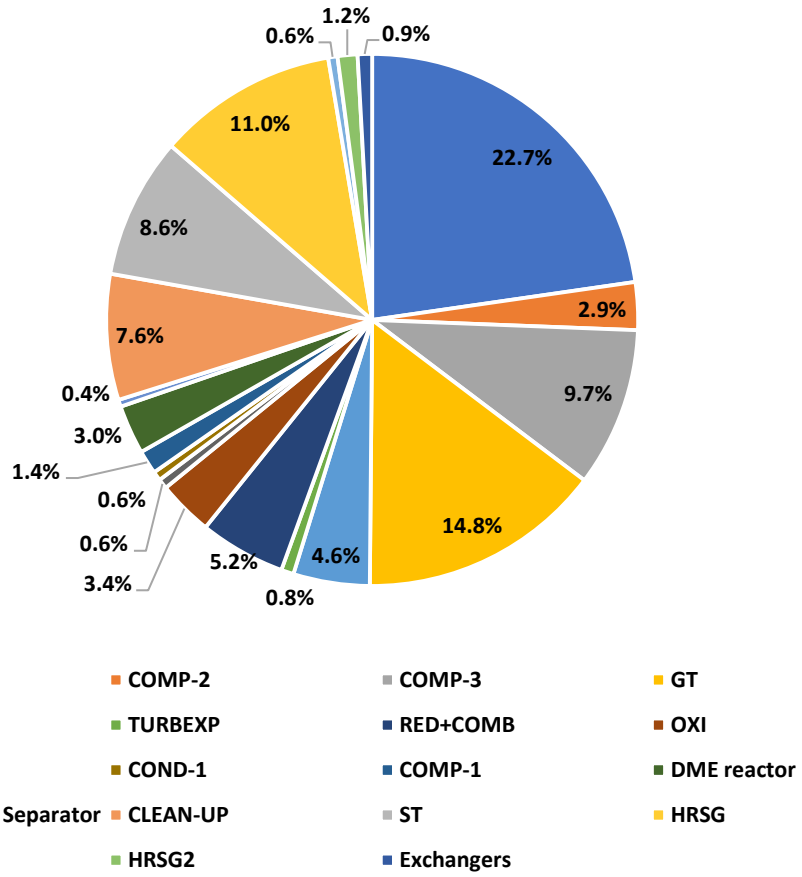

Figure 15 Contribution of the components to the TOC.

Finally, to evaluate the profitability of the plant during its lifetime a discounted cash flow analysis (DCF) was adopted. DCF is based on the concept of the time value of money, all the future cash flows are estimated and discounted by a discounted factor (i) (Table S8 in supplementary file), obtaining their present value [99]. The sum of the all discounted cash flows, both positive (revenues) and negative (operation cost, Table S7 in supplementary file), gives the net present values (NPV) as shown by equation (36).

$$\mathrm{NPV} = -\mathrm{TASC} + \sum_{l=1}^{\mathrm{t}} \frac{(\text{net cash flows})_l}{(1+\mathrm{i})^l} \qquad (36)$$

A project is acceptable only if the NPV is positive. TASC is used to evaluate the total project cost instead of TOC, in order to asses both escalation and interest during construction (Table S7 in supplementary file) [95,96]. A sensitivity analysis was performed to evaluate the effect of the selling price of power and DME on the economic performance of the plant.

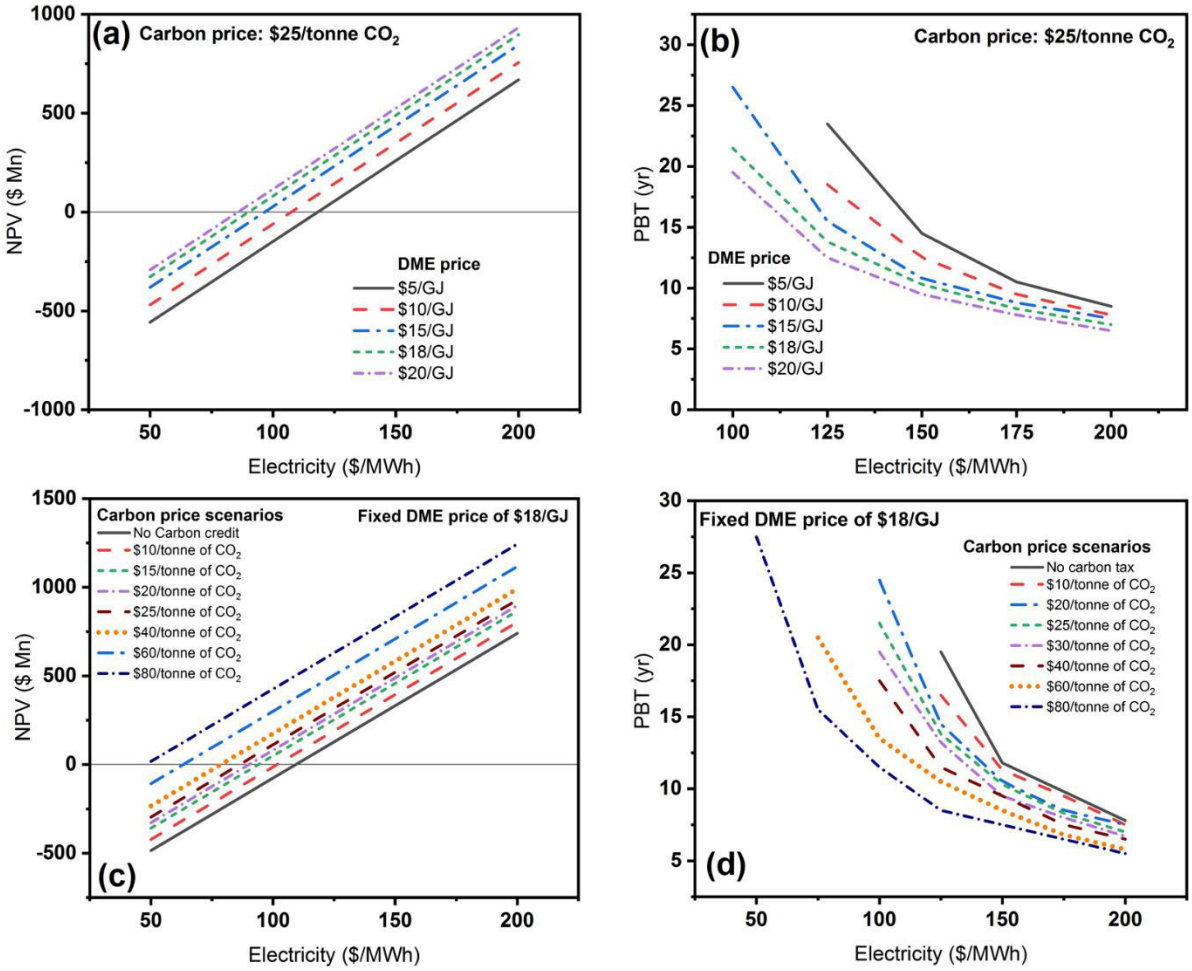

Figure 16 (a) and (c) Economic performance varying carbon credits and DME prices for different electricity prices (b) and (d) Payback period (PBT) varying DME and electricity price for different levels of carbon credit

It is observed that a payback period (PBT) of 20 years was obtained with the electricity and the selling price of DME of \$20/GJ and \$220/MWh respectively which is around 2.2 times the current whole sale electricity price without carbon credits considered

Figure 16 (a) and (b) represents the variation of electricity prices for different DME prices from \$5-20/GJ. It is observed that for the current reported carbon credit price of \$25/tonne of CO_2 [100] the NPV is positive if the electricity price of \$90/MWh (which is below current electricity price with CCS) with a payback period of 21.5 years. Nonetheless, a rapid increase in the CO_2 price between \$40 and \$80 per tonne is required to meet the agreements of Paris 2015 [101]. This trend can be observed in many countries where high carbon tax of over 55\$/tonne prevails including Switzerland, Finland, Sweden, Liechtenstein, Norway, Mexico, Chile and many others [101]. Indeed, such rapid rise in the carbon price have already started to materialize, with further increase to be seen developed economies by 2030 [102–105]. Still many developing countries are struggling to adopt the carbon price and emission trading system making it difficult to match the carbon price difference. Therefore, the NPV values was varied for different scenarios of electricity and DME price based on the carbon credit variation from \$10-80/tonne of CO_2 [106]. Figure 16 (c) and (d) corresponds to the fixed current market DME price of \$18/GJ [53] and varying the carbon credits for electricity pricing. From Figure 16 (c) it can be said with the carbon price above \$40/tonne CO_2 would have positive NPV that can be able to match with the current selling price of electricity is

above $100/MWh with carbon capture [106–111] for the proposed polygeneration with a PBT of 17.5 years, with potential to drop further for higher carbon credit scenarios of $60 and $80/tonne of CO_2 the payback period reduces by nearly 2/3 (11.5 years).

However, more strong carbon credit policies and a further development of technologies, such as Oxyfuel combustion, air separation, and chemical looping, will make the proposed polygeneration plant more competitive. By considering oxygen transport reactors that use ion transport membranes, such as perovskites, for oxygen separation at high temperatures (i.e., above 700^{o}C), high-purity oxygen could be produced at a relatively lower price compared to ASU, thereby increasing the efficiency and decreasing the equipment cost. At present, with this technology, it is possible to produce 2000 tonne per day, which is sufficient for an oxyfuel plant of 110 MW capacity. Therefore, with the adoption of the ion transport membrane technology that costs 31% less compared to the ASU, consequently, the cost of DME and power production would decrease tremendously and the overall efficiency of the plant would improve by 2-4% [112].

8. Conclusion

A novel natural gas feed polygeneration plant was proposed that integrates a chemical looping CO_2/H_2O splitting unit with an oxyfuel combustion unit for the production of power, DME and methanol. The results demonstrated the advantages of using a chemical looping CO_2/H_2O process in a polygeneration plant to reduce the efficiency penalty due to the carbon capture. The analysis revealed that the ideal H_2/CO ratio for a single step DME synthesis to be which can be obtained by feeding H_2O/CO_2 ratio of 60/40%. The plant was able to produce 103 MWe and 185.6 ton/day (2.15 kg/s) of DME with an energetic and exergetic efficiency of 50.2% and 45.0%, respectively. Compared to only power plant with carbon capture the present polygeneration revealed an efficiency gain of 4%. Through an exergy analysis, the main contributors of exergy destruction were identified: the combustor and reduction system resulted to contribute for 51.2% of the total generated irreversibilities (221 MW). The capital investment was estimated to be $534 million. The overall CO_2 produced was 3.36 million tonne for 7446 hours (with a capacity factor of 0.85) of annual operation of which approximately 3.4% is contributed by the DME production in a polygeneration scheme accounting for 589.15 kilotonne of total CO_2 avoided annually. Economic analysis revealed that around 23% of the total equipment costs is attributed by ASU and with the use of more sophisticated technology for producing oxygen at less price would decrease the capital investment. A discounted cash flow analysis revealed that the proposed plant would able to meet the electricity and DME price of $100/MWh an $18/GJ with the carbon credit of $40/tonne of CO_2, which is projected to be the carbon credit by 2020. With stringent carbon pricing of $80/tonne of CO_2 the electricity price would drop below $50/MWh.

Author Contributions:

A Farooqui and F Di Tomaso developed the model and performed simulations. A Farooqui, F Di Tomaso, A Bose and D Ferrero written the manuscript in multiple iterations. J Llorca and M Santarelli supervised the work and made the necessary modifications required in the manuscript. The figures were made in multiple iterations by A Farooqui and Di Tomaso.

Glossary:

$\dot{m}$	Mass flow rate (kg/s)
LHV	Lower heating value (MJ/kg)
W_{NET}	Net power produced inside the plant (MW)
W_{ST1}	Power produced in steam turbine of SRC1 (MW)
W_{ST2}	Power produced in steam turbine of SRC2 (MW)
W_{GT}	Power produced in gas turbine (MW)
$W_{COMP,tot}$	Auxiliary compression power in compressors (MW)
W_{COMP-3}	Auxiliary compression power for recycling CO_2 (MW)
$CO_{2,DME}$	CO_2 embedded in DME (%)
$CO_{2,REC}$	CO_2 recycled within the plant (%)
E	Total exergy (MW)
E_k	Kinetic exergy
E_{ph}	Physical exergy
E_{pot}	Potential exergy
E_{ch}	Chemical exergy
x	Mass fraction (-)
h	Mass enthalpy (kJ/kg)
s	Mass entropy (kJ/kg-K)
φ	Activity coefficient for the i-th component
R	Ideal gas constant (8.314 J/mol-K)
ρ	Density (kg/m^3)
p_{00}	Partial pressure of the i-th component (Pa)
W	Absorbed/produced work by the device (MW)
Q	Work obtained from heat flux (MW)
$I_{destroyed}$	Irreversibility generated (MW)
T	Temperature (^oC)
η_{ex}	Exergy efficiency (-)
η_c	Energy efficiency (-)
Q^*	Exergy obtainable using the heat of the selected stream
C_{equ}	Equipment cost
$C_{equ,actual}$	Actual component cost
$C_{equ,ref}$	Reference component cost
M	Scaling factor (-)
l	Number of years (-)
i	Discounted factor (-)
P	Pressure (bar)
χ	Relative irreversibilities
θ	Fuel depletion rate (%)
ξ	Productivity lack (%)
ψ	Exergetic factor (%)
P_0	Pressure at environment state of 1 atm
T_0	Temperature at environment state of 20^oC
E^0	Standard chemical exergy
ΔG^0	Gibbs free energy
e_{ch}	Specific chemical exergy (kJ/kg)
K_i	equilibrium constant ($m^3/kmol$)
k_i	Arrhenius rate constant

r	reaction rate (kmol/kg_{cat} s)
Π	concentration expressed (kmol/m^3)
B	activation energy (J/mol)
Pre	pre-exponential factor
RGIBBS	GIBBS Reactor where the calculations are based on minimizing the Gibbs energy
OC	Oxygen Carrier
C_{eff}	Plant carbon efficiency

Subscripts

ph	physical
ch	chemical
vap	vapor state
liq	liquid state
COMP	compression work
TURBEXP	work by turbo expansion
0	environment state of 1 atm and 20^{o}C
is	isentropic compressor
mech	mechanical
comp	compressor
turb	turbine
ex	exergy
in,i	contribution to inlet mass flows
out,i	contribution to outlet mass flows
tot	total or cumulative
i	i-th component in the mixture
COND	condenser
REB	reboiler
k	k-th component
P	product stream
F	resource stream

Acronyms

NG	Natural Gas
VLS	Vapor Liquid Seperator
CLN	Column
SRC	Steam Rankine Cycles
MR	Methane Reduction
WS	Water Splitting
CDS	Carbon dioxide Splitting
DME	Dimethyl Ether
ASU	Air Separation Unit
TURBOEXP	Turbo Expander
RED	Reduction Reactor
OXI	Oxidation Reactor
LHHW	Langmuir-Hinshelwood Hougen-Watson
ST	Steam Turbine
GT	Gas Turbine

PHX	Preheater
TPC	Total Project Cost
BEC	Bare Erected Cost
EPCC	Engineering, Procurement, Construction Cost
TOC	Total Overnight cost
TASC	Total As-spent cost
TPC	Total Project cost
NETL	National Energy Technology Laboratories
CEPCI	Chemical Engineering Plant Cost Index
OPEX	Operational Expenditure
CAPEX	Capital Expenditure
DCF	Discounted Cash Flow
NPV	Net Present Value
HR	Heat Rate
CSP	Concentrating Solar Power
CCS	Carbon Capture and Sequestration
PBT	Payback period in years

REFERENCES:

[1] I.E.A. IEA, CO2 Emissions from Fuel Combustion 2017 - Highlights, Int. Energy Agency. 1 (2017) 1–162. doi:10.1787/co2_fuel-2017-en.

[2] IPCC, IPCC special report on global warming of 1.5oC, 2019. http://www.ipcc.ch/report/sr15/.

[3] P. Viebahn, D. Vallentin, S. Höller, Prospects of carbon capture and storage (CCS) in China's power sector - An integrated assessment, Appl. Energy. 157 (2015) 229–244. doi:10.1016/j.apenergy.2015.07.023.

[4] M.E. Boot-Handford, J.C. Abanades, E.J. Anthony, M.J. Blunt, S. Brandani, N. Mac Dowell, J.R. Fernández, M.-C. Ferrari, R. Gross, J.P. Hallett, R.S. Haszeldine, P. Heptonstall, A. Lyngfelt, Z. Makuch, E. Mangano, R.T.J. Porter, M. Pourkashanian, G.T. Rochelle, N. Shah, J.G. Yao, P.S. Fennell, Carbon capture and storage update, Energy Environ. Sci. 7 (2014) 130–189. doi:10.1039/C3EE42350F.

[5] R.P. Cabral, N. Mac Dowell, A novel methodological approach for achieving £/MWh cost reduction of CO2 capture and storage (CCS) processes, Appl. Energy. 205 (2017) 529–539. doi:10.1016/j.apenergy.2017.08.003.

[6] Y. Zhao, B. Jin, Z. Deng, Y. Huang, X. Luo, Z. Liang, Thermodynamic analysis of a new chemical looping process for syngas production with simultaneous CO2capture and utilization, Energy Convers. Manag. 171 (2018) 1685–1696. doi:10.1016/j.enconman.2018.06.101.

[7] Q. Zhang, Nurhayati, C.L. Cheng, D. Nagarajan, J.S. Chang, J. Hu, D.J. Lee, Carbon capture and utilization of fermentation CO2: Integrated ethanol fermentation and succinic acid production as an efficient platform, Appl. Energy. 206 (2017) 364–371. doi:10.1016/j.apenergy.2017.08.193.

[8] C. Graves, S.D. Ebbesen, M. Mogensen, K.S. Lackner, Sustainable hydrocarbon fuels by recycling CO2 and H2O with renewable or nuclear energy, Renew. Sustain. Energy Rev. 15

(2011) 1–23. doi:10.1016/j.rser.2010.07.014.

[9] S.M. Jarvis, S. Samsatli, Technologies and infrastructures underpinning future CO2value chains: A comprehensive review and comparative analysis, Renew. Sustain. Energy Rev. 85 (2018) 46–68. doi:10.1016/j.rser.2018.01.007.

[10] A.E. Farooqui, M.A. Habib, H.M. Badr, R. Ben-Mansour, Modeling of ion transport reactor for oxy-fuel combustion, Int. J. Energy Res. 37 (2013). doi:10.1002/er.2923.

[11] R. Ben-Mansour, M.A. Habib, H.M. Badr, F. Azharuddin, M. Nemitallah, Characteristics of oxy-fuel combustion in an oxygen transport reactor, in: Energy and Fuels, ACS Publications, 2012: pp. 4599–4606. doi:10.1021/ef300539c.

[12] A. Farooqui, A. Bose, D. Ferrero, J. Llorca, M. Santarelli, Techno-economic and exergetic assessment of an oxy-fuel power plant fueled by syngas produced by chemical looping CO2 and H2O dissociation, J. CO2 Util. 27 (2018) 500–517. doi:10.1016/j.jcou.2018.09.001.

[13] K. Jana, A. Ray, M.M. Majoumerd, M. Assadi, S. De, Polygeneration as a future sustainable energy solution – A comprehensive review, Appl. Energy. 202 (2017) 88–111. doi:10.1016/j.apenergy.2017.05.129.

[14] Y.K. Salkuyeh, T.A. Adams, A new power, methanol, and DME polygeneration process using integrated chemical looping systems, Energy Convers. Manag. 88 (2014) 411–425. doi:10.1016/j.enconman.2014.08.039.

[15] S. Li, L. Gao, H. Jin, Realizing low life cycle energy use and GHG emissions in coal based polygeneration with CO2 capture, Appl. Energy. 194 (2017) 161–171. doi:10.1016/j.apenergy.2017.03.021.

[16] A. Bose, K. Jana, D. Mitra, S. De, Co-production of power and urea from coal with CO2 capture: Performance assessment, Clean Technol. Environ. Policy. 17 (2015) 1271–1280. doi:10.1007/s10098-015-0960-7.

[17] K. Jana, S. De, Environmental impact of biomass based polygeneration – A case study through life cycle assessment, Bioresour. Technol. 227 (2017) 256–265. doi:10.1016/j.biortech.2016.12.067.

[18] H. Huang, S. Yang, P. Cui, Design concept for coal-based polygeneration processes of chemicals and power with the lowest energy consumption for CO2capture, Energy Convers. Manag. 157 (2018) 186–194. doi:doi.org/10.1016/j.enconman.2017.11.073.

[19] Y.K. Salkuyeh, T.A. Adams, A new power, methanol, and DME polygeneration process using integrated chemical looping systems, Energy Convers. Manag. 88 (2014) 411–425. doi:10.1016/j.enconman.2014.08.039.

[20] R. Stanger, T. Wall, R. Spörl, M. Paneru, S. Grathwohl, M. Weidmann, G. Scheffknecht, D. McDonald, K. Myöhänen, J. Ritvanen, S. Rahiala, T. Hyppänen, J. Mletzko, A. Kather, S. Santos, Oxyfuel combustion for CO2capture in power plants, Int. J. Greenh. Gas Control. 40 (2015) 55–125. doi:10.1016/j.ijggc.2015.06.010.

[21] V.N. Nguyen, L. Blum, Syngas and synfuels from H2O and CO2: Current status, Chemie-Ingenieur-Technik. 87 (2015) 354–375. doi:10.1002/cite.201400090.

[22] G.P. Smestad, A. Steinfeld, Review: Photochemical and thermochemical production of solar fuels from H 2O and CO 2 using metal oxide catalysts, Ind. Eng. Chem. Res. 51 (2012) 11828–11840. doi:10.1021/ie3007962.

[23] B. Moghtaderi, Review of the recent chemical looping process developments for novel energy and fuel applications, Energy and Fuels. 26 (2012) 15–40. doi:10.1021/ef201303d.

[24] N. Saithong, S. Authayanun, Y. Patcharavorachot, A. Arpornwichanop, Thermodynamic analysis of the novel chemical looping process for two-grade hydrogen production with CO2 capture, Energy Convers. Manag. 180 (2019) 325–337. doi:10.1016/j.enconman.2018.11.003.

[25] C. Agrafiotis, M. Roeb, C. Sattler, A review on solar thermal syngas production via redox pair-based water/carbon dioxide splitting thermochemical cycles, Renew. Sustain. Energy Rev. 42 (2015) 254–285. doi:10.1016/j.rser.2014.09.039.

[26] D. Yadav, R. Banerjee, A review of solar thermochemical processes, Renew. Sustain. Energy Rev. 54 (2016) 497–532. doi:10.1016/j.rser.2015.10.026.

[27] P.T. Krenzke, J.R. Fosheim, J.H. Davidson, Solar fuels via chemical-looping reforming, Sol. Energy. 156 (2017) 48–72. doi:10.1016/j.solener.2017.05.095.

[28] S. Chuayboon, S. Abanades, S. Rodat, Syngas production via solar-driven chemical looping methane reforming from redox cycling of ceria porous foam in a volumetric solar reactor, Chem. Eng. J. 356 (2018) 756–770. doi:10.1016/j.cej.2018.09.072.

[29] A.E. Farooqui, A.M. Pica, P. Marocco, D. Ferrero, A. Lanzini, S. Fiorilli, J. Llorca, M. Santarelli, Assessment of kinetic model for ceria oxidation for chemical-looping CO2 dissociation, Chem. Eng. J. 346 (2018) 171–181. doi:10.1016/j.cej.2018.04.041.

[30] F. Liu, Cerium oxide promoted oxygen carrier development and scale modeling study for chemical looping comustion, University of Kentucky, 2013. https://uknowledge.uky.edu/cgi/viewcontent.cgi?article=1029&context=me_etds.

[31] K.J. Warren, J.R. Scheffe, Kinetic insights into the reduction of ceria facilitated via the partial oxidation of methane, Mater. Today Energy. 9 (2018) 39–48. doi:10.1016/j.mtener.2018.05.001.

[32] J. Kim, C.A. Henao, T.A. Johnson, D.E. Dedrick, J.E. Miller, E.B. Stechel, C.T. Maravelias, Methanol production from CO2 using solar-thermal energy: process development and techno-economic analysis, Energy Environ. Sci. 4 (2011) 3122. doi:10.1039/c1ee01311d.

[33] J. Kim, T.A. Johnson, J.E. Miller, E.B. Stechel, C.T. Maravelias, Fuel production from CO2 using solar-thermal energy: system level analysis, Energy Environ. Sci. 5 (2012) 8417. doi:10.1039/c2ee21798h.

[34] C. Falter, V. Batteiger, A. Sizmann, Climate Impact and Economic Feasibility of Solar Thermochemical Jet Fuel Production, Environ. Sci. Technol. 50 (2016) 470–477. doi:10.1021/acs.est.5b03515.

[35] T.C. Davenport, C.K. Yang, C.J. Kucharczyk, M.J. Ignatowich, S.M. Haile, Maximizing fuel production rates in isothermal solar thermochemical fuel production, Appl. Energy. 183 (2016) 1098–1111. doi:10.1016/j.apenergy.2016.09.012.

[36] C. Falter, R. Pitz-Paal, Energy analysis of solar thermochemical fuel production pathway with a focus on waste heat recuperation and vacuum generation, Sol. Energy. 176 (2018) 230–240. doi:10.1016/J.SOLENER.2018.10.042.

[37] S.H. Park, C.S. Lee, Applicability of dimethyl ether (DME) in a compression ignition engine as an alternative fuel, Energy Convers. Manag. 86 (2014) 848–863. doi:10.1016/j.enconman.2014.06.051.

[38] E. Catizzone, G. Bonura, M. Migliori, F. Frusteri, G. Giordano, CO2 recycling to dimethyl ether: State-of-the-art and perspectives, Molecules. 23 (2018) 1–28. doi:10.3390/molecules23010031.

[39] W. Ying, L. Genbao, Z. Wei, Z. Longbao, Study on the application of DME/diesel blends in a diesel engine, Fuel Process. Technol. 89 (2008) 1272–1280. doi:10.1016/j.fuproc.2008.05.023.

[40] A. Bakhtyari, M.R. Rahimpour, Methanol to Dimethyl Ether, in: A. Basile, F. Dalena (Eds.), Methanol Sci. Eng., Elsevier B.V., 2017: pp. 281–311. doi:10.1016/B978-0-444-63903-5.00010-8.

[41] T. Ogawa, N. Inoue, T. Shikada, Y. Ohno, Direct Dimethyl Ether Synthesis, J. Nat. Gas Chem. 12 (2003) 219–227.

[42] T.A. Semelsberger, R.L. Borup, H.L. Greene, Dimethyl ether (DME) as an alternative fuel, J. Power Sources. 156 (2006) 497–511. doi:10.1016/j.jpowsour.2005.05.082.

[43] Department of Energy and Climate Change, DECC Fossil Fuel Price Projections, London, 2013.

[44] W.B. Group, Commodity Markets Outlook, Washington, DC, 2018. doi:10.1017/CBO9781107415324.004.

[45] G. M, K. R, J. E, Production of methanol and dimethyl ether from biomass derived syngas: a comparison of the different synthesis pathways by means of flowsheet simulation, in: 23rd Eur. Symp. Comput. Aided Process Eng. (ESCAPE 23) 9-12 June, 2013, 2013: p. 2013. doi:10.1016/B978-0-7506-3560-8.50001-9.

[46] F. Ren, J.-F. Wang, H.-S. Li, Direct mass production technique of dimethyl ether from synthesis gas in a circulating slurry bed reactor, Stud. Surf. Sci. Catal. 159 (2006) 489–492. https://www.scopus.com/inward/record.uri?eid=2-s2.0-33745792734&partnerID=40&md5=25145520ec4d439b01fe6100b67846b8.

[47] T.A. Adams, J.H. Ghouse, Polygeneration of fuels and chemicals, Curr. Opin. Chem. Eng. 10 (2015) 87–93. doi:10.1016/j.coche.2015.09.006.

[48] K. Saravanan, H. Ham, N. Tsubaki, J.W. Bae, Recent progress for direct synthesis of dimethyl ether from syngas on the heterogeneous bifunctional hybrid catalysts, Appl. Catal. B Environ. 217 (2017) 494–522. doi:10.1016/j.apcatb.2017.05.085.

[49] A. Hankin, N. Shah, Process exploration and assessment for the production of methanol and dimethyl ether from carbon dioxide and water, Sustain. Energy Fuels. 00 (2017) 1–16. doi:10.1039/C7SE00206H.

[50] K. Li, H. Wang, Y. Wei, Syngas generation from methane using a chemical-looping concept: A review of oxygen carriers, J. Chem. (2013). doi:10.1155/2013/294817.

[51] D.R. Simbeck, A.D. Karp, R.L. Dickenson, Syngas production for gas-to-liquids applications: Technologies, issues and outlook., 1998. https://web.anl.gov/PCS/acsfuel/preprint archive/Files/Merge/Vol-45_1-0003.pdf.

[52] S. Luo, L. Zeng, D. Xu, M. Kathe, E. Chung, N. Deshpande, L. Qin, A. Majumder, T.L. Hsieh, A. Tong, Z. Sun, L.S. Fan, Shale gas-to-syngas chemical looping process for stable shale gas conversion to high purity syngas with a H2:CO ratio of 2:1, Energy Environ. Sci. 7 (2014) 4104–4117. doi:10.1039/c4ee02892a.

[53] A. Lerner, M.J. Brear, J.S. Lacey, R.L. Gordon, P.A. Webley, Life cycle analysis (LCA) of low emission methanol and di-methyl ether (DME) derived from natural gas, Fuel. 220 (2018) 871–878. doi:10.1016/j.fuel.2018.02.066.

[54] H.M. Shim, S.J. Lee, Y.D. Yoo, Y.S. Yun, H.T. Kim, Simulation of DME synthesis from coal syngas by kinetics model, Korean J. Chem. Eng. 26 (2009) 641–648. doi:10.1007/s11814-009-0107-9.

[55] G.H. Graaf, J.G.M. Winkelman, Chemical Equilibria in Methanol Synthesis Including the Water-Gas Shift Reaction: A Critical Reassessment, Ind. Eng. Chem. Res. 55 (2016) 5854–5864. doi:10.1021/acs.iecr.6b00815.

[56] M.K. Cohce, I. Dincer, M.A. Rosen, Energy and exergy analyses of a biomass-based hydrogen production system, Bioresour. Technol. 102 (2011) 8466–8474. doi:10.1016/j.biortech.2011.06.020.

[57] A.M. Eltony, H.G. Park, S.X. Wang, J. Kong, I.L. Chuang, Motional heating in a graphene-coated ion trap, Nano Lett. 14 (2014) 5712–5716. doi:10.1021/nl502468g.

[58] D.-Y. Peng, D.B. Robinson, A New Two-Constant Equation of State, Ind. Eng. Chem. Fundam. 15 (1976) 59–64. doi:10.1021/i160057a011.

[59] L. Fanxing, Z. Liang, V.L. G., Y. Zachary, F. Liang-Shih, Syngas chemical looping gasification process: Bench-scale studies and reactor simulations, AIChE J. 56 (2009) 2186–2199. doi:10.1002/aic.12093.

[60] I. Barin, Thermochemical data of pure substances, (1995) 1885. doi:10.1002/9783527619825.

[61] M.B. Berkenpas, J.J. Fry, K. Kietzke, E.S. Rubin, IECM User Documentation : User Manual IECM User Documentation : User Manual, (2018) 509–515.

[62] CAESAR project - European best practice guidelines for assessment of CO2 capture technologies., 2011. https://www.sintef.no/globalassets/project/decarbit/d-1-4-3_euro_bp_guid_for_ass_co2_cap_tech_280211.pdf.

[63] M.N. Khan, T. Shamim, Influence of Specularity Coefficient on the Hydrodynamics and Bubble Statistics of an Annular Fluidized Bed Reactor, Energy Procedia. 105 (2017) 1998–2003. doi:10.1016/j.egypro.2017.03.573.

[64] D.K. Bhunya, Simulation Study of Cryogenic Air Separation Unit Using Aspen Hysys At Rourkela Steel Plant Master of Technology in (Cryogenic and Vacuum Technology) National Institute of Technology Rourkela, National Institute of Technology Rourkela, 2014. http://ethesis.nitrkl.ac.in/5971/1/E-138.pdf.

[65] J. Aprilia, K. Kolmetz, Air seperation units (Engineering design guideline) KLM Technology Group-Practical Engineering Guidelines for Processing Plant Solutions, 2013. http://kolmetz.com/pdf/EDG/ENGINEERING_DESIGN_GUIDELINE_Air_Seperation_Units_Rev01web.pdf.

[66] V. Raibhole, S. Sapali, Simulation of Medium Purity Gaseous Oxygen Cryogenic Plant for Biomass Gasification by Aspen Plus, Open Access Sci. Reports. 1:343 (2012). doi:10.4172/scientificreports.343.

[67] B.J.P. Buhre, L.K. Elliott, C.D. Sheng, R.P. Gupta, T.F. Wall, Oxy-fuel combustion technology for coal-fired power generation, Prog. Energy Combust. Sci. 31 (2005) 283–307. doi:10.1016/j.pecs.2005.07.001.

[68] D. Cocco, A. Pettinau, G. Cau, Energy and economic assessment of IGCC power plants integrated with DME synthesis processes, Proc. Inst. Mech. Eng. Part A J. Power Energy. 220 (2006) 95–102. doi:10.1243/095765006X76027.

[69] S. Mukherjee, P. Kumar, A. Yang, P. Fennell, Energy and exergy analysis of chemical looping combustion technology and comparison with pre-combustion and oxy-fuel combustion technologies for CO2 capture, J. Environ. Chem. Eng. 3 (2015) 2104–2114. doi:10.1016/j.jece.2015.07.018.

[70] Y. Khojasteh-Salkuyeh, New Polygeneration Processes for Power Generation and Liquid Fuel Production with Zero CO2 Emissions, McMaster University, 2015.

[71] M. Pozzo, A. Lanzini, M. Santarelli, Enhanced biomass-to-liquid (BTL) conversion process through high temperature co-electrolysis in a solid oxide electrolysis cell (SOEC), Fuel. 145 (2015) 39–49. doi:10.1016/j.fuel.2014.12.066.

[72] K.L. Ng, D. Chadwick, B.A. Toseland, Kinetics and modelling of dimethyl ether synthesis from synthesis gas, Chem. Eng. Sci. 54 (1999) 3587–3592. doi:10.1016/S0009-2509(98)00514-4.

[73] F. Dadgar, R. Myrstad, P. Pfeifer, A. Holmen, H.J. Venvik, Direct dimethyl ether synthesis from synthesis gas: The influence of methanol dehydration on methanol synthesis reaction, Catal. Today. 270 (2016) 76–84. doi:10.1016/j.cattod.2015.09.024.

[74] C. Arcoumanis, C. Bae, R. Crookes, E. Kinoshita, The potential of di-methyl ether (DME) as an alternative fuel for compression-ignition engines: A review, Fuel. 87 (2008) 1014–1030. doi:10.1016/j.fuel.2007.06.007.

[75] J. Sun, G. Yang, Y. Yoneyama, N. Tsubaki, Catalysis chemistry of dimethyl ether synthesis, ACS Catal. 4 (2014) 3346–3356. doi:10.1021/cs500967j.

[76] R.S. Treptow, Le Chatelier's Principle, J. Chem. Educ. 57 (1980) 417–419. doi:10.1021/ed057p417.

[77] F. Pontzen, W. Liebner, V. Gronemann, M. Rothaemel, B. Ahlers, CO2-based methanol and DME - Efficient technologies for industrial scale production, Catal. Today. 171 (2011) 242–250. doi:10.1016/j.cattod.2011.04.049.

[78] M. Tobiszewski, M. Marć, A. Gałuszka, J. Namiešnik, Green chemistry metrics with special reference to green analytical chemistry, Molecules. 20 (2015) 10928–10946. doi:10.3390/molecules200610928.

[79] A. Hankin, N. Shah, Process exploration and assessment for the production of methanol and dimethyl ether from carbon dioxide and water, in: A. Basile, F. Dalena (Eds.), Methanol Sci. Eng., Elsevier B.V., 2017: pp. 1541–1556. doi:10.1039/C7SE00206H.

[80] M.C. Gutiérrez, J.M. Rosas, M.A. Rodríguez-Cano, I. López-Luque, J. Rodríguez-Mirasol, T. Cordero, Strategic situation, design and simulation of a biorefinery in Andalusia, Energy Convers. Manag. 182 (2019) 201–214. doi:10.1016/j.enconman.2018.12.038.

[81] K.M. Vanden Bussche, G.F. Froment, A Steady-State Kinetic Model for Methanol Synthesis and the Water Gas Shift Reaction on a Commercial Cu/ZnO/Al2O3Catalyst, J. Catal. 161 (1996) 1–10. doi:10.1006/jcat.1996.0156.

[82] G. Berčič, J. Levec, Catalytic Dehydration of Methanol to Dimethyl Ether. Kinetic Investigation and Reactor Simulation, Ind. Eng. Chem. Res. 32 (1993) 2478–2484. doi:10.1021/ie00023a006.

[83] R.S. Schiffino, R.P. Merrill, A mechanistic study of the methanol dehydration reaction on .gamma.-alumina catalyst, J. Phys. Chem. 97 (1993) 6425–6435. doi:10.1021/j100126a017.

[84] G.W. K. Klier, Simmons, Catalytic Synthesis of Methanol from CO / H2, J. Catal. 360 (1982) 343–360. doi:https://doi.org/10.1016/0021-9517(82)90040-9.

[85] G.R. Moradi, F. Yaripour, P. Vale-Sheyda, Catalytic dehydration of methanol to dimethyl ether over mordenite catalysts, Fuel Process. Technol. 91 (2010) 461–468. doi:10.1016/j.fuproc.2009.12.005.

[86] O. Y, S. T, O. T, O. M, M. M, F. K, New Clean Fuel from Coal-Dimethyl Ether, in: 213th ACS Natl. Meet. San Fr., 1997: pp. 1–5.

[87] D.Y.C. Leung, G. Caramanna, M.M. Maroto-Valer, An overview of current status of carbon dioxide capture and storage technologies, Renew. Sustain. Energy Rev. 39 (2014) 426–443. doi:10.1016/j.rser.2014.07.093.

[88] A.D. Curzons, D.J.C. Constable, D.N. Mortimer, V.L. Cunningham, So you think your process is green, how do you know? - Using principles of sustainability to determine what is green - A corporate perspective, Green Chem. 3 (2001) 1–6. doi:10.1039/b007871i.

[89] R.A. Sheldon, Metrics of Green Chemistry and Sustainability: Past, Present, and Future, ACS Sustain. Chem. Eng. 6 (2018) 32–48. doi:10.1021/acssuschemeng.7b03505.

[90] I.C. Kemp, Pinch analysis and process integration: A user guide on process integration for the efficient use of energy, Pinch Anal. Process Integr. (2007) 416. doi:http://dx.doi.org/10.1016/B978-075068260-2.50003-1.

[91] T.J. Kotas, Chapter 2 - Basic exergy concepts BT - The Exergy Method of Thermal Plant Analysis, in: Butterworth-Heinemann, 1985: pp. 29–56. doi:https://doi.org/10.1016/B978-0-408-01350-5.50009-X.

[92] A.P. Hinderink, F.P.J.M. Kerkhof, A.B.K. Lie, J. De Swaan Arons, H.J. Van Der Kooi, Exergy analysis with a flowsheeting simulator - I. Theory; calculating exergies of material streams, Chem. Eng. Sci. 51 (1996) 4693–4700. doi:10.1016/0009-2509(96)00220-5.

[93] J.Y. Xiang, M. Cal, M. Santarelli, Calculation for physical and chemical exergy of flows in systems elaborating mixed-phase flows and a case study in an IRSOFC plant, 115 (2004) 101–115. doi:10.1002/er.953.

[94] J. Szargut, Chemical Exergies of the Elements, Appl. Energy. 32 (1989) 269–286.

[95] Kristen Gerdes, John Haslbeck, Norma Kuehn, Eric Lewis, Lora L. Pinkerton, Mark Woods, James Simpson, Marc J. Turner, Elsy Varghese, Cost and Performance Baseline for Fossil Energy Plants Volume 1: Bituminous Coal and Natural Gas to Electricity, Doe/Netl-2010/1397. 1 (2010). doi:DOE/NETL-2010/1397.

[96] K. Gerdes, W.M. Summers, J. Wimer, Cost Estimation Methodology for NETL Assessments of Power Plant Performance, Doe/Netl-2011/1455. (2011) 26. http://www.netl.doe.gov/File Library/research/energy analysis/publications/QGESSNETLCostEstMethod.pdf.

[97] J.A.S. Richard Turton, Richard C. Bailie, Wallace B. Whiting, Analysis, Synthesis and Design of Chemical Processes Third Edition, 2013. doi:10.1017/CBO9781107415324.004.

[98] Politecnico di Milano - CAESER Project, Enabling advanced pre-combustion capture techniques and plants; in deliverable D.1.4.3: European best practice guidelines for assessment of CO2 capture technologies, 2011.

https://www.sintef.no/globalassets/project/decarbit/d-1-4-3_euro_bp_guid_for_ass_co2_cap_tech_280211.pdf.

[99] M. Yang, International Energy Agency Working Paper Series Modeling Investment Risks and Uncertainties with Real Options Approach Modeling Investment Risks and Uncertainties with Real Options Approach, Structure. 13 (2007) 1120–37. http://www.iea.org/Textbase/publications/free_new_Desc.asp?PUBS_ID=1857.

[100] F. Watson, EU CO2 price to hit Eur30/mt by end 2019: Bank of America, Spglobal.Com. (2018). https://www.spglobal.com/platts/en/market-insights/videos/market-movers-europe/112618-oil-price-decline-takes-center-stage (accessed December 4, 2018).

[101] World Bank Group, State and Trends of Carbon Pricing 2018, Washington, DC, 2018. doi:10.1596/978-1-4648-1292-7.

[102] S. Ambrogi, EU carbon prices could double by 2021 and quadruple by 2030, Https://Www.Carbontracker.Org. (2018). https://www.carbontracker.org/eu-carbon-prices-could-double-by-2021-and-quadruple-by-2030/ (accessed December 4, 2018).

[103] Z. Said, A.A. Alshehhi, A. Mehmood, Predictions of UAE's renewable energy mix in 2030, Renew. Energy. 118 (2018) 779–789. doi:10.1016/j.renene.2017.11.075.

[104] J. Bordoff, N. Kaufman, A Federal US Carbon Tax: Major Design Decisions and Implications, Joule. 2 (2018) 2487–2491. doi:10.1016/j.joule.2018.11.020.

[105] K.C. de Bruin, A.M. Yakut, The Economic and Environmental Impacts of Increasingarbon tax the Irish Carbon Tax: The Economic and Social Research Institute., 2018. doi:https://doi.org/10.26504/rs79.

[106] B. Dolter, N. Rivers, The cost of decarbonizing the Canadian electricity system, Energy Policy. 113 (2018) 135–148. doi:10.1016/j.enpol.2017.10.040.

[107] The Full Costs of Electricity Provision; NEA No. 7298: Nuclear Energy Agency, Organisation for economic co-operation and development, 2018. http://www.oecd-nea.org/ndd/pubs/2018/7298-full-costs-2018.pdf.

[108] A. Mezősi, L. Szabó, S. Szabó, Cost-efficiency benchmarking of European renewable electricity support schemes, Renew. Sustain. Energy Rev. 98 (2018) 217–226. doi:10.1016/j.rser.2018.09.001.

[109] M. Johannes, T. Jessica, H. Niklas, S. Charlotte, P. Simon, N. Sebastian, L. Simon, S. Noha, S. Thomas, K. Christoph, Levelized Cost of Electricity Renewable Energy Technologies: Fraunhofer ISE, 2013. www.ise.fraunhofer.de.

[110] N. Gal, I. Milstein, A. Tishler, C.K. Woo, Investment in electricity capacity under fuel cost uncertainty: Dual-fuel and a mix of single-fuel technologies, Energy Policy. 126 (2019) 518–532. doi:10.1016/j.enpol.2018.10.040.

[111] Executive summary: Projected costs of generating electricity, 2015. doi:10.1007/s00247-002-0666-y.

[112] P.N. Dyer, R.E. Richards, S.L. Russek, D.M. Taylor, Ion transport membrane technology for oxygen separation and syngas production, Solid State Ionics. 134 (2000) 21–33. doi:10.1016/S0167-2738(00)00710-4.

[113] R. Dindorf, Estimating potential energy savings in compressed air systems, Procedia Eng. 39 (2012) 204–211. doi:10.1016/j.proeng.2012.07.026.